Euro. Jnl of Applied Mathematics (1999), *vol.* 10, *pp.* 185–220. Printed in the United Kingdom

Thermal stress analysis and homogenization for catalytic combustor monoliths

S. T. KOLACZKOWSKI[1], P. LIN[2], A. B. MOVCHAN[3], S. K. SERKOV[2], and A. SPENCE[2]

[1] *School of Chemical Engineering, University of Bath, Bath BA2 7AY, UK*
[2] *Department of Mathematical Sciences, University of Bath, Bath BA2 7AY, UK*
[3] *Department of Mathematical Sciences, University of Liverpool, Liverpool, L69 3BX, UK*

(*Received 9 May 1997: revised 3 April 1998*)

We present a simple and rigorous mathematical model and efficient numerical algorithm for the three-dimensional thermal stress analysis of composite structures used in high-temperature catalytic combustors. Numerical experiments are carried out for three types of cell geometries. A homogenization algorithm is implemented, and asymptotic formulae are derived for the effective elastic moduli of the periodic structures.

1 Introduction

Catalytic combustion is a primary combustion process where the combustor, say in a conventional gas turbine, is replaced by catalytic section(s) [1]. In this paper, we present a mathematical model developed for the thermal stress analysis in a catalytic combustor monolith. This is a honeycomb type of structure, consisting of a large number of parallel channels in which the gas flows. The walls of the channels are coated with a catalyst that enables flameless combustion reactions of lean fuel-air mixtures to be initiated and sustained, at lower temperatures (500–1200 °C) than would otherwise be possible in a conventional combustor. The diameter of the channels is of the order of 1 mm and the wall thickness is about 0.1 mm.

As the combustion reactions occur in, or in proximity to, the catalyst-coated walls in the monolith, then at any fixed position the temperature of the wall is greater than that of the gas. In the direction of gas flow down the channel, both gas and wall temperature continue to increase until all of the reactants have been consumed. A detailed description of these processes is available elsewhere [2]. In an ideal situation, it would be desirable to maintain a uniform temperature, chemical composition and velocity profile at the inlet and across the face of the catalytic monolith, so that the reactions subsequently proceed in each channel in a similar manner. In practice this is difficult to achieve. This then has the effect of causing differences in temperature to exist between neighbouring channels, which when combined with temperature gradients in the direction of gas flow may lead to unacceptable thermal stresses and fracture of the monolith. As new materials with high coefficients of thermal expansion have been developed for high temperature catalytic combustion regions, this problem has become more serious [3].

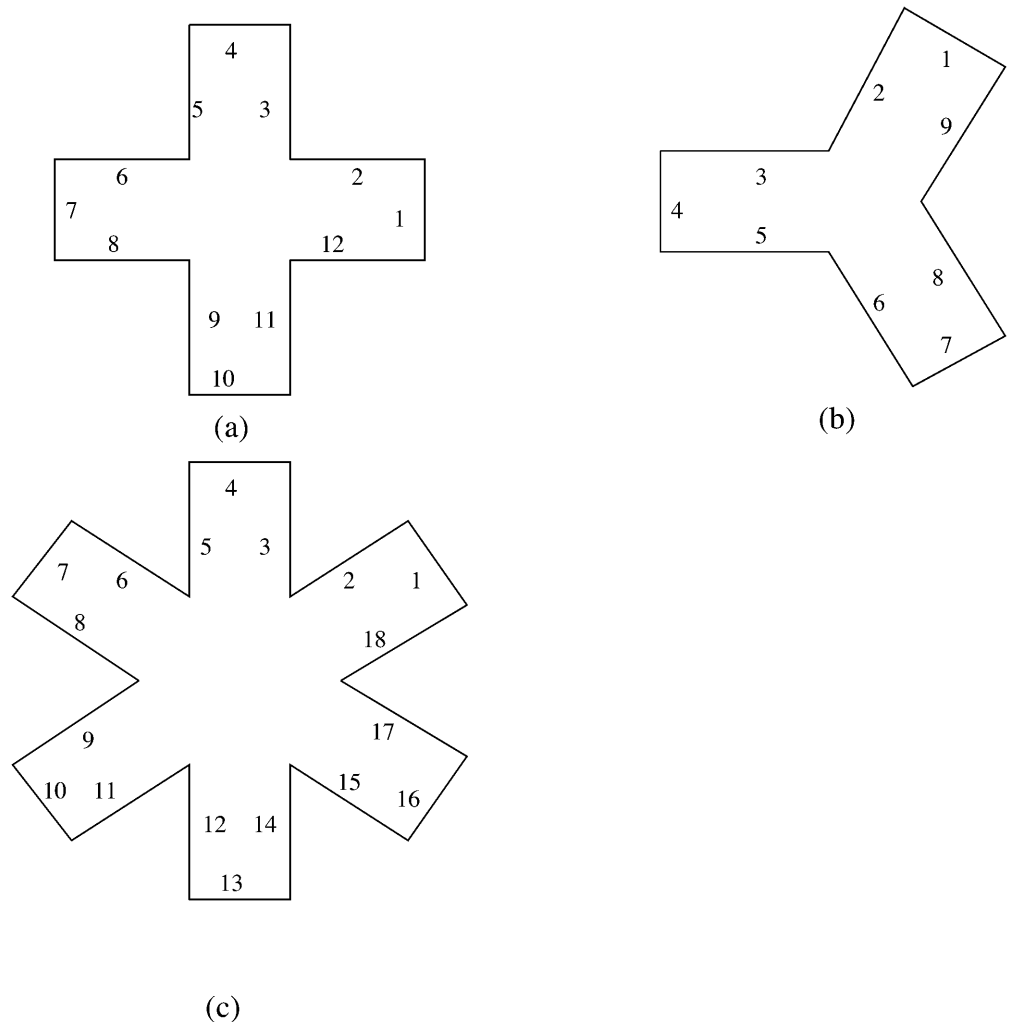

FIGURE 1. Cross-sections of junctions between the cells.

Extensive studies of elastic and thermal properties of two-dimensional catalytic combustor monoliths have also been discussed [3–6]. Various two-dimensional finite element codes have been successfully used to generate the data for this analysis. We remark that the use of two-dimensional codes is good only under the assumption that the physical properties such as temperature and pressure, as well as elastic properties of the materials are constant along each channel. This is not the case when the combustion along the channel is taken into consideration, where a full three-dimensional model is required.

We present analytical and numerical results for the three-dimensional modelling of thermal stresses in catalytic combustor monoliths, where the size of an elementary cell is considerably smaller than the length of the channel. This motivates us to extend the asymptotic analysis for elastic 'thin' structures [7] to formulations of uncoupled thermoelasticity.

https://doi.org/10.1017/S0956792599003654 Published online by Cambridge University Press

Although catalytic monoliths may involve a great variety of prismatic geometries, we will only study structures whose cells have *square, triangular* or *hexagonal* cross-sections. Specifically, we apply our asymptotic analysis to finite cylinders with three types of cross sections shown in Fig. 1. In Fig. 1, the *cross-shaped* region corresponds to the square cell geometry of the honeycomb, the *Y-shaped* region corresponds to the hexagonal cell geometry, and the remaining third case corresponds to the case of a triangular cell. Further, we present the results of homogenization of structures whose elementary cells are shown in Fig. 16. The asymptotic algorithm used in this work enables us to evaluate accurately the effective moduli of the honeycomb structures. In particular, it is important for the cases when the effective shear moduli are small and the direct application of the finite element method does not provide sufficient accuracy.

2 Governing equations

In this section, we describe the basic model. It is essential that combustion in the catalytic combustor monolith occurs at a relatively low temperature compared to the standard combustor without a catalyst. For this case, the equations of linear elasticity provide an appropriate model that gives a good agreement with experiment. We refer to the work [4] produced at Rolls Royce IMGT, where a linear two-dimensional finite element analysis was presented as a simple numerical model matching nicely with the results of experiments. In our work we consider fully three-dimensional field and develop an asymptotic approach which proves to be more efficient than the finite element method. The equations come from the theory of linear uncoupled thermoelasticity. For detailed description and classification of problems of thermoelasticity we refer to Nowacki [8]. We consider only those cases where the materials of which catalytic monoliths are made are isotropic and homogeneous.

Suppose that at some temperature T_0, the elastic body is undeformed (with no external forces present). Due to the action of external forces (i.e. body force and surface tractions), the action of internal heat sources and the heat flux through the surface, the elastic solid undergoes a deformation which is accompanied by nonzero displacements and a temperature increment $\theta = T - T_0$. Assuming that the elastic strain and the relative change of temperature θ/T_0 are small we reduce the governing equations to a system of linear equations of equilibrium and the heat conduction equation. We shall study a steady state problem, and a reasonable approximation for the solution will be obtained as a result of analysis of equations of uncoupled thermo-elasticity.

The equations of equilibrium are

$$\sum_{j=1}^{3} \frac{\partial}{\partial x_j} \sigma_{ij} + f_i = 0, \quad i = 1, 2, 3, \tag{1}$$

where σ_{ij} are components of the stress tensor, u_i are components of the vector of displacement $\mathbf{u}$ and f_i are components of the body force density $\mathbf{f}$.

The constitutive relations of thermoelasticity give the expressions of the components of the stress tensor in terms of strain components and temperature θ. They are assumed to be

$$\sigma_{ij} = 2\mu\varepsilon_{ij} + \left(\lambda \sum_{k=1}^{3} \varepsilon_{kk} - \gamma\theta \right) \delta_{ij}, \tag{2}$$

https://doi.org/10.1017/S0956792599003654 Published online by Cambridge University Press

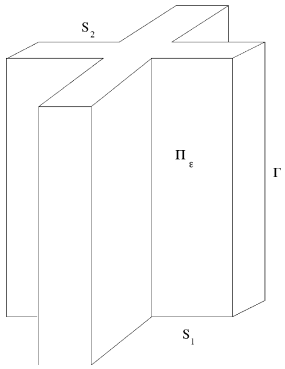

FIGURE 2. A finite cylinder corresponding to the junction region in the monolith structure.

where

$$\varepsilon_{ij} = \frac{1}{2}\left(\frac{\partial}{\partial x_j}u_i + \frac{\partial}{\partial x_i}u_j\right), \tag{3}$$

$$\delta_{ij} = 1, \quad \text{if } i = j; \quad \delta_{ij} = 0, \quad \text{if } i \neq j.$$

In (2), λ and μ are the elastic moduli and

$$\gamma = (3\lambda + 2\mu)\,\alpha,$$

with α being the coefficient of linear thermal expansion.

When the model problem is static and the body forces and sources of heat vanish, the system of equations of uncoupled thermoelasticity has the form

$$\mu\nabla^2\mathbf{u} + (\lambda + \mu)\nabla\nabla\cdot\mathbf{u} = \gamma\nabla\theta, \tag{4}$$

$$\nabla^2\theta = 0. \tag{5}$$

We assume Dirichlet boundary conditions for the temperature and mixed Dirichlet–Neumann conditions for components of the displacement vector, as follows. Let

$$\Pi_\varepsilon = \{\mathbf{x};\, 0 < x_3 < l,\, \varepsilon^{-1}(x_1, x_2) \in G \subset \mathbb{R}^2\}$$

represent the junction area in the monolith structure, where ε is a small positive non-dimensional parameter, and G is a bounded domain with Lipschitz boundary. Let Γ denote the lateral surface of Π_ε, and let S_1, S_2 be the end regions (as indicated in Fig. 2).

The temperature is assumed to be given on the boundary of Π_ε:

$$\theta|_\Gamma = \Theta(x_1/\varepsilon,\, x_2/\varepsilon, x_3), \tag{6}$$

$$\theta|_{S_i} = \Theta^{(i)}, \quad i = 1, 2. \tag{7}$$

The boundary conditions for the elastic displacement field are specified as follows:

$$\mathbf{u}|_{S_2} = \mathbf{0}, \tag{8}$$

$$\boldsymbol{\sigma}^{(3)}(\mathbf{u})|_{S_1} = \mathbf{0}, \tag{9}$$

$$\boldsymbol{\sigma}^{(n)}|_\Gamma = \varepsilon^2\mathbf{P}(\mathbf{x}, \mathbf{n}), \tag{10}$$

where $\mathbf{n}$ is the outward normal to Γ.

https://doi.org/10.1017/S0956792599003654 Published online by Cambridge University Press

The boundary conditions (8), (9) mean that the end region S_1 is free of tractions and the end region S_2 is fixed; the boundary condition (10) specifies pressure on the lateral surface Γ (the pressure is allowed to change within the combustor monolith).

For problems of *uncoupled* thermoelasticity we deal first with the boundary value problem for the Laplace equation (5) and calculate the temperature. We then analyse the boundary value problem for the Navier system (4) and find the displacement and stress field. In the following section we describe an efficient and accurate asymptotic procedure; we remark that it does not require large computer resources and, therefore, has obvious advantages in comparison with numerical technique based on, say, three-dimensional finite element algorithms.

3 Asymptotic analysis

In this section, we introduce and discuss the asymptotic algorithm developed for analysis of boundary value problems in thin cylindrical domains with cross-sections associated with junctions. The asymptotic analysis used is an extension of the results [9].

3.1 Three-dimensional distribution of temperature

We briefly describe the asymptotic procedure to solve the Laplace equation (5) with the boundary conditions (6), (7). Let us first introduce the notation

$$\zeta = (\zeta_1, \zeta_2) = \varepsilon^{-1}(x_1, x_2), \quad z = x_3. \tag{11}$$

We shall use an asymptotic series of the form

$$\theta \sim \sum_{k=0}^{\infty} \varepsilon^{2k}\, \theta_k(\zeta_1, \zeta_2, z). \tag{12}$$

It follows that θ_0 satisfies the two-dimensional Dirichlet problem

$$\nabla_\zeta^2\, \theta_0 = 0, \quad \zeta \in S; \quad \theta_0|_{\partial S} = \Theta(\zeta_1, \zeta_2, z), \tag{13}$$

where S is the scaled cross-section, and $\theta_k, k \geqslant 1$, satisfies

$$\nabla_\zeta^2\, \theta_k + \frac{\partial^2 \theta_{k-1}}{\partial z^2} = 0, \quad \zeta \in S; \quad \theta_k|_{\partial S} = 0.$$

We notice that $\theta_0(\zeta_1, \zeta_2, z)$ does not necessarily satisfy the boundary conditions (7) on S_1 and S_2, if $z = 0, l$, respectively. This problem is resolved by adding boundary layers. We construct the boundary layer $\tau_0^{(1)}(\mathbf{X})$ near S_1 by defining

$$\mathbf{X} = (\mathbf{X}_1, \mathbf{X}_2, \mathbf{X}_3); \quad \mathbf{X}_i = x_i/\varepsilon, \quad i = 1, 2, 3, \tag{14}$$

and

$$\Pi^{(1)} = \{\mathbf{X};\, (\mathbf{X}_1, \mathbf{X}_2) \in G,\, 0 \leqslant \mathbf{X}_3 < \infty\}, \quad \text{(semi-infinite cylinder)},$$

$$\Gamma^{(1)} = \{\mathbf{X};\ \mathbf{X} \in \partial\Pi^1,\, \mathbf{X}_3 > 0\}, \quad \text{(lateral surface)},$$

$$\Gamma^{(2)} = \{\mathbf{X};\, \mathbf{X} \in \partial\Pi^1,\, \mathbf{X}_3 = 0\}, \quad \text{(bottom region)}.$$

https://doi.org/10.1017/S0956792599003654 Published online by Cambridge University Press

In order for $\theta_0 + \tau_0^{(1)}$ to satisfy the Laplace equation and the boundary condition, $\tau_0^{(1)}(\mathbf{X})$ needs to satisfy the following three-dimensional Dirichlet problem

$$\nabla_{\mathbf{X}}^2 \tau_0^{(1)} = 0, \quad \mathbf{X} \in \Pi^{(1)} \tag{15}$$

$$\tau_0^{(1)}|_{\Gamma^{(1)}} = 0, \quad \tau_0^{(1)}|_{\Gamma^{(2)}} = \Theta^{(1)} - \Theta(\mathbf{X}_1, \mathbf{X}_2, 0). \tag{16}$$

To provide matching between the outer and inner expansions of the total field in a neighbourhood of the end region, we seek a solution of (15), (16) with finite energy; such a solution exists (see Maz'ya *et al.* [10]) and it decays exponentially at infinity.

A similar argument applies to the construction of the boundary layer $\tau_0^{(2)}(\mathbf{Y})$ near S_2, where

$$\mathbf{Y} = (\mathbf{Y}_1, \mathbf{Y}_2, \mathbf{Y}_3); \quad \mathbf{Y}_1 = x_1/\varepsilon, \mathbf{Y}_2 = x_2/\varepsilon, \mathbf{Y}_3 = \frac{x_3 - l}{\varepsilon}, \tag{17}$$

and it also follows that the contribution to the interior from the boundary layer is exponentially small.

3.2 Polynomial solutions of the homogeneous boundary value problem

The numerical algorithm will use polynomial (in the longitudinal variable) solutions of a homogeneous model problem for the Navier system in an infinite cylinder; we refer to Arutyunyan *et al.* [11] and Shkalikov & Shkred [12]. We are looking for non-trivial solutions of the following homogeneous boundary value problem

$$\mu\nabla^2 \mathbf{U}(\boldsymbol{\zeta}, z) + (\lambda + \mu)\nabla\nabla \cdot \mathbf{U}(\boldsymbol{\zeta}, z) = \mathbf{0}, \quad (\boldsymbol{\zeta}, z) \in \Pi, \tag{18}$$

$$\boldsymbol{\sigma}^n(\mathbf{U}; (\boldsymbol{\zeta}, z)) := \boldsymbol{\sigma}(\mathbf{U}, (\boldsymbol{\zeta}, z))\,\mathbf{n} = \mathbf{0}, \quad (\boldsymbol{\zeta}, z) \in \partial\Pi, \tag{19}$$

where $\Pi = \{(\boldsymbol{\zeta}, z) : z \in (-\infty, \infty), \boldsymbol{\zeta} = (\zeta_1, \zeta_2) \in G \subset \mathbb{R}^2\}$, and G is a bounded domain with Lipschitz boundary. For the sake of convenience, it is also assumed that the principal inertia axes of G coincide with the coordinate axes, i.e.

$$\int_G \zeta_1\, d\zeta_1\, d\zeta_2 = 0, \quad \int_G \zeta_2\, d\zeta_1\, d\zeta_2 = 0, \quad \int_G \zeta_1\, \zeta_2\, d\zeta_1\, d\zeta_2 = 0.$$

It is shown (see Arutyunyan *et al.* [11] and the Appendix) that any solution $\mathbf{U}$ can be represented as a linear combination of 12 vector functions:

$$\sum_{j=0}^{L} \frac{z^j}{j!}\, \boldsymbol{\phi}^{(k,L-j)}(\zeta_1, \zeta_2), \tag{20}$$

$$\text{for } k = 1, 2,\ L = 0, 1, 2, 3; \quad \text{or for } k = 2, 3,\ L = 0, 1,$$

where the functions $\boldsymbol{\phi}^{(k,L-j)}(\zeta_1, \zeta_2)$ are given in Appendix A.1.

3.3 Asymptotic approximation. The Navier operator

This section deals with the asymptotic procedure for a mixed boundary value problem for the Navier operator in the thin cylinder Π_ε.

The boundary value problem (4), (8), (9), (10) can be represented in the matrix form,

https://doi.org/10.1017/S0956792599003654 Published online by Cambridge University Press

using (11)

$$\mathbf{L}(\partial_{\zeta_1}, \partial_{\zeta_2}, \partial_z)\,\mathbf{u} = -\varepsilon^2\,\mathbf{F}, \quad \text{in } \Pi_\varepsilon, \tag{21}$$

$$\mathbf{T}(\partial_{\zeta_1}, \partial_{\zeta_2}, \mathbf{n})\,\mathbf{u} = \varepsilon^3\,\mathbf{P}, \quad \text{on } \Gamma, \tag{22}$$

$$\mathbf{u}|_{z=l} = \mathbf{0}, \tag{23}$$

$$\sigma^{(3)}(\mathbf{u})|_{z=0} = \mathbf{0}, \tag{24}$$

where $-\mathbf{F}$ is the right-hand side of (4),

$$\mathbf{L} = \mathbf{L}_0(\partial_{\zeta_1}, \partial_{\zeta_2}) + \varepsilon\mathbf{L}_1(\partial_{\zeta_1}, \partial_{\zeta_2})\,\frac{d}{dz} + \varepsilon^2\,\mathbf{L}_2\frac{d^2}{dz^2}, \tag{25}$$

$$\mathbf{T} = \mathbf{T}_0(\partial_{\zeta_1}, \partial_{\zeta_2}, \mathbf{n}) + \varepsilon\mathbf{T}_1(\mathbf{n})\,\frac{d}{dz}, \tag{26}$$

$$\mathbf{L}_0 = \begin{pmatrix} (2\mu+\lambda)\,\partial_{\zeta_1}^2 + \mu\partial_{\zeta_2}^2 & (\mu+\lambda)\,\partial_{\zeta_1}\partial_{\zeta_2} & 0 \\ (\mu+\lambda)\,\partial_{\zeta_1}\partial_{\zeta_2} & (2\mu+\lambda)\,\partial_{\zeta_2}^2 + \mu\partial_{\zeta_1}^2 & 0 \\ 0 & 0 & \mu(\partial_{\zeta_1}^2 + \partial_{\zeta_1}^2) \end{pmatrix},$$

$$\mathbf{L}_1 = (\lambda+\mu)\begin{pmatrix} 0 & 0 & \partial_{\zeta_1} \\ 0 & 0 & \partial_{\zeta_2} \\ \partial_{\zeta_1} & \partial_{\zeta_2} & 0 \end{pmatrix}; \quad \mathbf{L}_2 = \begin{pmatrix} \mu & 0 & 0 \\ 0 & \mu & 0 \\ 0 & 0 & (2\mu+\lambda) \end{pmatrix},$$

$$\mathbf{T}_0 = n_1\begin{pmatrix} (2\mu+\lambda)\,\partial_{\zeta_1} & \lambda\partial_{\zeta_2} & 0 \\ \mu\partial_{\zeta_2} & \mu\partial_{\zeta_1} & 0 \\ 0 & 0 & \mu\partial_{\zeta_1} \end{pmatrix} + n_2\begin{pmatrix} \mu\partial_{\zeta_2} & \mu\partial_{\zeta_1} & 0 \\ \lambda\partial_{\zeta_1} & (2\mu+\lambda)\,\partial_{\zeta_2} & 0 \\ 0 & 0 & \mu\partial_{\zeta_2} \end{pmatrix},$$

$$\mathbf{T}_1 = \begin{pmatrix} 0 & 0 & \lambda n_1 \\ 0 & 0 & \lambda n_2 \\ \mu n_1 & \mu n_2 & 0 \end{pmatrix}.$$

It was proved [7] that the displacement field $\mathbf{u}$ in Π_ε can be approximated by the asymptotic series

$$\mathbf{u}(\mathbf{x}, \varepsilon) \sim \sum_{k=0}^{\infty} \varepsilon^k \{\boldsymbol{\Psi}^{(k)}(\zeta_1, \zeta_2, z, \varepsilon) + \mathbf{V}^{(1,k)}(\mathbf{X}_1, \mathbf{X}_2, \mathbf{X}_3, \varepsilon) + \mathbf{V}^{(2,k)}(\mathbf{Y}_1, \mathbf{Y}_2, \mathbf{Y}_3, \varepsilon)\}, \tag{27}$$

where $\boldsymbol{\Psi}^{(k)}$ represents the displacement outside the neighbourhoods of the end regions, $\mathbf{V}^{(i,k)}$are the boundary layers which provide the validity of the boundary conditions (23), (24) at the end regions, where we have used the notations (14), (17). As in the thermal problem, the boundary layer fields are specified in a semi-infinite cylinder, and they decay exponentially at infinity. To illustrate the algorithm, we construct the leading ansatz of the asymptotic series (27).

Theorem [7] *The vector-valued function*

$$\boldsymbol{\Psi}^{(0)}(\zeta, z, \varepsilon) = \sum_{k=1}^{2}\sum_{j=0}^{3} \varepsilon^j \frac{\partial^j}{\partial z^j}\, v_k(z)\,\boldsymbol{\phi}^{k,j}(\zeta) + \varepsilon^2 \sum_{k=3}^{4}\sum_{j=0}^{1} \varepsilon^j \frac{\partial^j}{\partial z^j}\, v_k(z)\,\boldsymbol{\phi}^{k,j}(\zeta) + \varepsilon^4\,\mathbf{U}(\zeta, z), \tag{28}$$

https://doi.org/10.1017/S0956792599003654 Published online by Cambridge University Press

satisfies the equation

$$\mu\nabla^2 \boldsymbol{\Psi}^{(0)}(\mathbf{x}) + (\lambda+\mu)\nabla\nabla\cdot\boldsymbol{\Psi}^{(0)}(\mathbf{x}) = -\varepsilon^2\,\mathbf{F}(\zeta, z) - \varepsilon^3\,\mathbf{F}^{(0)}(\zeta, z) - \varepsilon^4\,\mathbf{F}^{(1)}(\zeta, z),\ \mathbf{x}\in\Pi_\varepsilon, \quad (29)$$

and the traction boundary condition

$$\sigma^n(\boldsymbol{\Psi}^{(0)}, \mathbf{x}) := \sigma(\boldsymbol{\Psi}^{(0)}, \mathbf{x})\,\mathbf{n} = \varepsilon^3\,\mathbf{P}(\zeta, z) + \varepsilon^4\,\mathbf{P}^{(0)}(\zeta, z),\ (\zeta, z)\in\partial\Omega\times[0, l], \quad (30)$$

where v_k, $\mathbf{F}^{(0)}$, $\mathbf{F}^{(1)}$, $\mathbf{P}^{(0)}$ *are bounded.*

The functions used above are specified as follows:

(1) The vector-valued functions

$$\mathbf{F}(\zeta, z)\in C^\infty((L^2(\Omega))^3;\ [0, l]) \quad \text{and} \quad \mathbf{P}(\zeta, z)\in C^\infty((L^2(\partial\Omega))^3;\ [0, l])$$

are given.

(2) $v_k(\cdot)$ are the solutions of the following ordinary differential equations:

$$\frac{d^4}{dz^4}\,v_k(z) = \frac{1}{D_k}\left(\int_\Omega F_k(\zeta, z)\,d\zeta + \int_{\partial\Omega} P_k(\zeta, z)\,ds\right), \quad k = 1, 2, \quad (31)$$

$$\frac{d^2}{dz^2}\,v_3(z) = -\frac{1}{D_3}\left(\int_\Omega F_3(\zeta, z)\,d\zeta + \int_{\partial\Omega} P_3(\zeta, z)\,ds\right), \quad (32)$$

$$\frac{d^2}{dz^2}\,v_4(z) = -\frac{1}{D_4}\left(\int_\Omega (\zeta_1 F_2(\zeta, z) - \zeta_2 F_1(\zeta, z))\,d\zeta + \int_{\partial\Omega} (\zeta_1 P_2(\zeta, z) - \zeta_2 P_1(\zeta, z))\,ds\right), \quad (33)$$

where

$$D_k = \mu\frac{2\mu+3\lambda}{\lambda+\mu}\int_\Omega \zeta_k^2\,d\zeta, \quad k = 1, 2,$$

$$D_3 = \mu\,\frac{2\mu+3\lambda}{\lambda+\mu}\,|\Omega|,$$

$$D_4 = \mu\int_\Omega ||\nabla\varphi - \zeta_2\,\mathbf{e}^{(1)} + \zeta_1\,\mathbf{e}^{(2)}||^2\,d\zeta.$$

We need to prescribe the boundary conditions in order to pose the boundary value problem for those four ordinary differential equations in (31)–(33). In our applications, we set in (23) and (24) that the left end of the cylinder is traction free, and that the right end is clamped. It has been shown [7] that the boundary layer terms $\mathbf{V}^{(1,k)}$ and $\mathbf{V}^{(2,k)}$ in (27) decay exponentially at infinity if and only if the following conditions are satisfied (consistently with the well-known St. Venant principle adopted in engineering models of elastic bars).

Zero Displacement (*including Zero Rotation Angles*) at $z = l$:

$$v_k(l) = 0, \quad \frac{dv_k}{dz}(l) = 0, \quad k = 1, 2; \quad v_k(l) = 0, \quad k = 3, 4. \quad (34)$$

Traction and Moment Free Surface at $z = 0$:

$$\frac{d^2 v_k}{dz^2}(0) = 0, \quad \frac{d^3 v_k}{dz^3}(0) = 0, \quad k = 1, 2, \quad \frac{dv_k}{dz}(0) = 0, \quad k = 3, 4. \quad (35)$$

https://doi.org/10.1017/S0956792599003654 Published online by Cambridge University Press

The boundary value problems for the vector functions $\mathbf{V}^{(1,k)}$, $\mathbf{V}^{(2,k)}$ are presented in Appendix A.2 for $k = 0$.

(3) For each fixed $z \in [0, l]$, the vector function $\mathbf{U}$ satisfies the two-dimensional boundary value problem

$$-\mathbf{L}_0\mathbf{U} = \mathbf{F}(\zeta, z) + \mathbf{L}_1\left(\frac{d^4 v_1}{dz^4}\boldsymbol{\phi}^{(1,3)} + \frac{d^4 v_2}{dz^4}\boldsymbol{\phi}^{(2,3)} + \frac{d^2 v_3}{dz^2}\boldsymbol{\phi}^{(3,1)} + \frac{d^2 v_4}{dz^2}\boldsymbol{\phi}^{(4,1)}\right)$$
$$+\mathbf{L}_2\left(\frac{d^4 v_1}{dz^4}\boldsymbol{\phi}^{(1,2)} + \frac{d^4 v_2}{dz^4}\boldsymbol{\phi}^{(2,2)} + \frac{d^2 v_3}{dz^2}\boldsymbol{\phi}^{(3,0)} + \frac{d^2 v_4}{dz^2}\boldsymbol{\phi}^{(4,0)}\right), \quad \zeta \in \Omega, \tag{36}$$

$$\mathbf{T}_0\,\mathbf{U} = \mathbf{P}(\zeta, z) - \mathbf{T}_1\left(\frac{d^4 v_1}{dz^4}\boldsymbol{\phi}^{(1,3)} + \frac{d^4 v_2}{dz^4}\boldsymbol{\phi}^{(2,3)} + \frac{d^2 v_3}{dz^2}\boldsymbol{\phi}^{(3,1)} + \frac{d^2 v_4}{dz^2}\boldsymbol{\phi}^{(4,1)}\right), \quad \zeta \in \partial\Omega. \tag{37}$$

(4) The vector-valued functions

$$\mathbf{F}^{(0)}(\zeta, z) \in C^\infty((L^2(\Omega))^3; [0, l]),\ \mathbf{F}^{(1)}(\zeta, z) \in C^\infty((L^2(\Omega))^3; [0, l])$$

and

$$\mathbf{P}^{(0)}(\zeta, z) \in C^\infty((L^2(\partial\Omega))^3; [0, l])$$

are chosen in a such a way that

$$\mathbf{F}^{(0)} = \sum_{k=1}^{2}\left\{\frac{d^5 v_k(z)}{dz^5}\,\mathbf{L}_2\,\varphi^{(k,3)} + \frac{d^3 v_{k+2}(z)}{dz^3}\,\mathbf{L}_2\,\varphi^{(k+2,1)}\right\} + \mathbf{L}_1\,\mathbf{U},$$

$$\mathbf{F}^{(1)} = \mathbf{L}_2\,\mathbf{U}, \quad \mathbf{P}^{(0)} = \mathbf{T}_1(\mathbf{n})\,\mathbf{U}.$$

3.4 Two-dimensional boundary value problem for the field U

To carry out the numerical experiments, we would like to make the following comments and simplifications which are essential to our application.

We note that the problem (36), (37) can be decomposed into a two-dimensional Neumann boundary value problem for the Navier operator coupled with a two-dimensional problem for the Poisson equation with the Neumann boundary condition, i.e.

$$\begin{pmatrix} (2\mu+\lambda)\,\partial_{\zeta_1}^2 + \mu\partial_{\zeta_2}^2 & (\mu+\lambda)\,\partial_{\zeta_1}\partial_{\zeta_2} \\ (\mu+\lambda)\,\partial_{\zeta_1} & (2\mu+\lambda)\,\partial_{\zeta_2}^2 + \mu\partial_{\zeta_1}^2 \end{pmatrix}\begin{pmatrix} U_1 \\ U_2 \end{pmatrix} = \begin{pmatrix} -f_1 \\ -f_2 \end{pmatrix}, \quad \zeta \in \Omega, \tag{38}$$

$$n_1\begin{pmatrix} (2\mu+\lambda)\,\partial_{\zeta_1} & \lambda\partial_{\zeta_2} \\ \mu\partial_{\zeta_2} & \mu\partial_{\zeta_1} \end{pmatrix}\begin{pmatrix} U_1 \\ U_2 \end{pmatrix} + n_2\begin{pmatrix} \mu\partial_{\zeta_2} & \mu\partial_{\zeta_1} \\ \lambda\partial_{\zeta_1} & (2\mu+\lambda)\,\partial_{\zeta_2} \end{pmatrix}\begin{pmatrix} U_1 \\ U_2 \end{pmatrix} = \begin{pmatrix} p_1 \\ p_2 \end{pmatrix}, \quad \zeta \in \partial\Omega, \tag{39}$$

and

$$(\partial_{\zeta_1}^2 + \partial_{\zeta_1}^2)\,U_3 = -f_3/\mu, \quad \zeta \in \Omega, \tag{40}$$

$$(n_1\,\partial_{\zeta_1} + n_2,\partial_{\zeta_1})\,U_3 = p_3/\mu, \quad \zeta \in \partial\Omega, \tag{41}$$

where U_i are the components of $\mathbf{U}$, f_i, p_i are the components of the right-hand side of (36) and (37), respectively.

The above equations are solvable, since the required orthogonality conditions for the

https://doi.org/10.1017/S0956792599003654 Published online by Cambridge University Press

right-hand sides are satisfied. In other words, we have

$$\int_\Omega f_i \, d\zeta - \int_{\partial\Omega} p_i \, ds = 0, \quad i = 1, 2, 3,$$

$$\int_\Omega (\zeta_1 f_2 - \zeta_2 f_1) \, d\zeta - \int_{\partial\Omega} (\zeta_1 p_2 - \zeta_2 p_1) \, ds = 0,$$

which are indeed consistent with (31), (32) and (33).

It follows from (4) that

$$-\varepsilon^2 \mathbf{F}(\zeta, z) = \gamma \nabla_{\mathbf{x}} \theta = \gamma \left(\varepsilon^{-1} \nabla_\zeta + \mathbf{e}^{(3)} \frac{d}{dz} \right) \theta. \tag{42}$$

Consider the traction boundary conditions. Since we consider the thermal stress, we must use the formula (2) for the stress tensor. Therefore, we have

$$\sum_{j=1}^{3} \sigma_{ij}^T n_j = \sigma_i^n - (\gamma\theta) n_i, \tag{43}$$

where

$$\sigma_i^n := \sum_{j=1}^{3} \left\{ 2\mu\varepsilon_{ij} + \lambda \sum_{k=1}^{3} \varepsilon_{kk} \, \delta_{i,j} \right\} n_j$$

is exactly the boundary traction in terms of the classical elasticity, or $\varepsilon^3 \mathbf{P} = \sigma^n$. In our numerical experiments, we assume that the boundary pressure p, a scalar function, is given and we shall regard the thermal boundary traction $\sigma_{i,j}^T n_j = -p n_i$. Hence,

$$\varepsilon^3 \mathbf{P} = \boldsymbol{\sigma}^n = -p\mathbf{n} + \gamma\theta\mathbf{n}.$$

Introduce the normalization

$$p = \varepsilon^3 \bar{p}, \quad \theta = \varepsilon^3 \bar{\theta}.$$

Substituting $\mathbf{F}$ and $\mathbf{P}$ into (31)–(33) and using the Divergence Theorem, we obtain that

$$\frac{d^4}{dz^4} v_k(z) = -\frac{1}{D_k} \int_{\partial\Omega} \bar{p} n_k(\zeta, z) \, ds, \quad k = 1, 2, \tag{44}$$

$$\frac{d^2}{dz^2} v_3(z) = \frac{\gamma}{D_3} \int_\Omega \frac{d}{dz} \bar{\theta} \, d\zeta, \tag{45}$$

$$\frac{d^2}{dz^2} v_4(z) = \frac{1}{D_4} \int_{\partial\Omega} (\zeta_1 \bar{p} n_2(\zeta, z) - \zeta_2 \bar{p} n_1(\zeta, z)) \, ds, \tag{46}$$

where we have used $n_3 = 0$.

4 Numerical implementation

In this section, we shall describe the numerical algorithm.

Step 1. The three auxiliary Neumann boundary value problems (A 6)–(A 8) for the Laplace equation are solved numerically by the NAG Laplace Solver *D03EAF*, so that we have the numerical solutions for the torsion and bending potentials φ, χ_1, χ_2.

https://doi.org/10.1017/S0956792599003654 Published online by Cambridge University Press

Step 2. In our numerical experiment, we assume that at the left entry point, i.e. at $z = 0$, the temperature varies between 1000 and 1200 °C, while at $z = l$, the right outflow point, the temperature is identically 1200 °C. The boundary values of the temperature at $z = 0$ are specified as follows:

Fig. 1(a):

$$\theta = \begin{cases} 1200\,^{\circ}\mathrm{C} & \text{on intervals 2–6} \\ 1000\,^{\circ}\mathrm{C} & \text{on intervals 8–12} \\ \text{linear approximation} & \text{on intervals 1, 7} \end{cases}$$

Fig. 1(b):

$$\theta = \begin{cases} 1200\,^{\circ}\mathrm{C} & \text{on intervals 8, 9} \\ 1000\,^{\circ}\mathrm{C} & \text{on intervals 2–6} \\ \text{linear approximation} & \text{on intervals 1, 7} \end{cases}$$

Fig. 1(c):

$$\theta = \begin{cases} 1200\,^{\circ}\mathrm{C} & \text{on intervals 8, 9, 17, 18} \\ 1000\,^{\circ}\mathrm{C} & \text{on intervals 2–6, 11–15} \\ \text{linear approximation} & \text{on intervals 1, 7, 10, 16} \end{cases}$$

The results of experiments [4] show that, to leading-order approximation, we can assume that the temperature on the lateral surface Γ of the channel depends linearly upon z. at each grid point $z = z_k$, On each cross-section $z = z_k$, we need to solve only a two-dimensional Dirichlet boundary value problem for the Laplace equation for the temperature θ by the same NAG Solver (see § 3.1).

Step 3. After Steps 1–2, we are able to calculate the set of functions $\{\boldsymbol{\phi}^{(k,j)}\}$ (see (A 5)), and the discretized temperature gradients. Then, both the right-hand sides of (36) and (37) are known at each grid point. We use the COSMOS/M program and the NAG Laplace Solver *D03EAF* to deal with the two-dimensional Navier system (38), (39) and the Poisson equation (40), (41).

Step 4. Given the boundary pressure, we can solve those four ordinary equations (44)–(46). To solve (45), the discretized temperature gradient in z is calculated with the use of data from Step 2.

With the above four steps, we are able to calculate the whole displacement vector $\boldsymbol{\Psi}^{(0)}$ (see (28)), which then leads to the evaluation of the stress components. We use the following values of the elastic moduli:

$$\text{Young's Modulus} = 3.0 \times 10^{10}\,(Pa),$$

$$\text{Poisson's ratio} = 0.25,$$

$$\text{Coefficient of linear thermal expansion} = 1.0 \times 10^{-6}(K^{-1}).$$

We set $l = 0.2$. We use a uniform mesh on the plane ζ, with the mesh size being 0.003. A uniform grid in z is also used, with the grid size being 0.004.

We present the results of two numerical tests.

(1) First, we demonstrate that the above asymptotic algorithm enables one to take into

https://doi.org/10.1017/S0956792599003654 Published online by Cambridge University Press

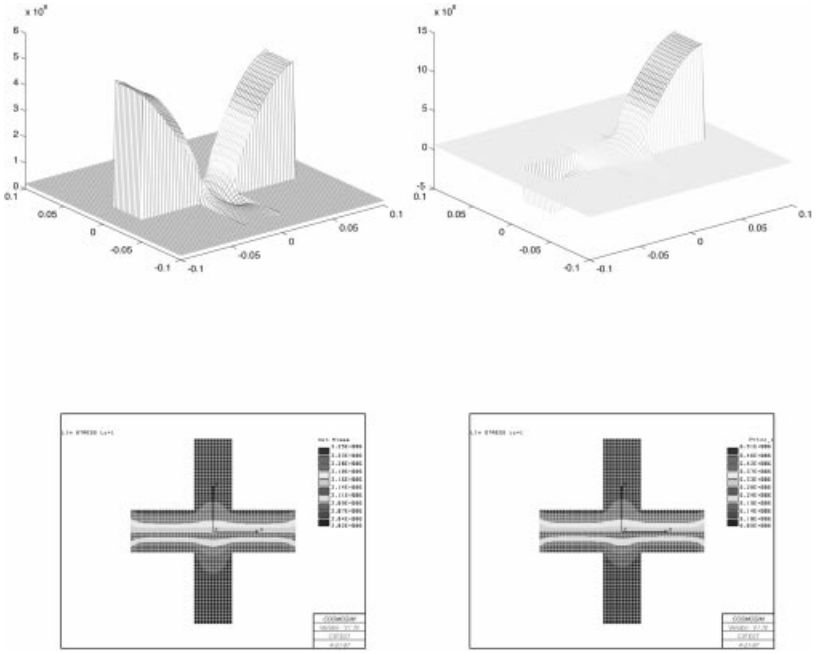

FIGURE 3. The cross-section (a); $z = 0.3l$. 3D graphs of the von Mises stress (top-left) and the greatest principal eigenvalue (top-right). 2D COSMOS/M contours of the the von Mises stress (bottom-left) and the greatest principal eigenvalue (bottom-right) for the field **U**. First numerical test.

account not only the longitudinal tension-compression (along the z-axis) but also bending. We set $\varepsilon = 0.1$ and assume that at $z = 0$ the pressure in the channels with the higher temperature (1200°C) is equal to $1.001 \times 10^6\ Pa$, whereas in the other channels (at $z = 0$) the pressure is assumed to be $10^6\ Pa$. At $z = l$ the pressure in all channels is equal to $1.025 \times 10^6\ Pa$, and the z-dependence of pressure in the channels is assumed to be linear.

(2) In the second numerical test we assume that in each cross-section the pressure is the same in all channels, but it varies linearly along the z-axis. At the left end ($z = 0$) we set the pressure to be $10^6\ Pa$, and at the left end ($z = l$) it is equal to $1.025 \times 10^6\ Pa$. The small parameter ε is set to be 0.01.

We emphasize that the numerical simulation is three-dimensional. To illustrate this we give the results for two separate cross sections at $z = 0.3l$ and $z = 0.7l$. The contour line pictures and the 3D surface pictures for the largest principal eigenvalue of the stress tensor and the von Mises stress

$$\sigma_{vonMises} := (\tfrac{1}{6}[(\sigma_1 - \sigma_2)^2 + (\sigma_1 - \sigma_3)^2 + (\sigma_2 - \sigma_3)^2])^{1/2}$$

with σ_i being the principal components of the stress tensor, are presented.

Figures 3–8 illustrate the results of the first numerical experiment (that involves bending) and include the data for the greatest principal stress and the von Mises stress for all three types of junctions shown in Fig. 1.

https://doi.org/10.1017/S0956792599003654 Published online by Cambridge University Press

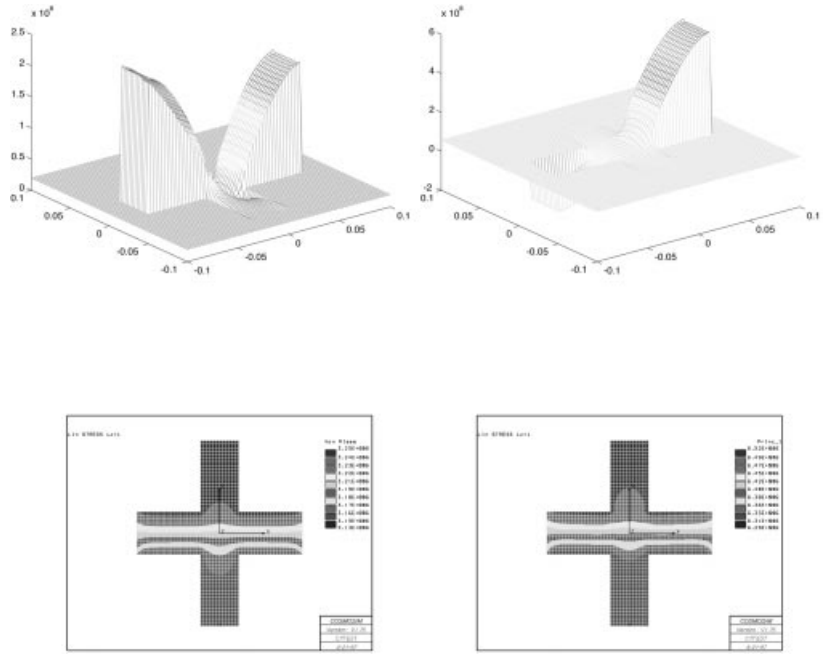

FIGURE 4. The cross-section (a); $z = 0.7l$. 3D graphs of the von Mises stress (top-left) and the greatest principal eigenvalue (top-right). 2D COSMOS/M contours of the the von Mises stress (bottom-left) and the greatest principal eigenvalue (bottom-right) for the field **U**. First numerical test.

In Figs 9–14, we illustrate the results for the second numerical test where we emphasize the contribution of the temperature gradient in the stress state.

The results of numerical computations show that the pressure and temperature difference may cause the stress concentration within the junction areas; in particular, the 2D pictures exhibit the stress concentration near the corners. It is explicit that the singular behaviour of stress is associated with solutions φ, χ_1, χ_2 of the auxiliary 2D problems (A6)–(A8) formulated on the scaled cross-section of the 3D junction; the surface plots show the behaviour of the total stress field produced by the full ansatz of the asymptotic expansion (35). One can see that the 3D model exhibits 'bending' of the junction area (Figs 3–6) caused by the pressure difference. In Figs 7–14, the pressure was self-balanced, and and the bending mode is not observed.

It is known (see Williams [13]) that, in general, the solutions of problems of linear elasticity may have singular stress components near the angular points of the boundary; the greatest order of singularity corresponds to the case (c) of Fig. 1, then we have the cross-section of Fig. 1(a), and the smallest exponent of singularity corresponds to the geometry in Fig. 1(b). In the next section, we also show that the effective shear moduli are small for the cell-structures corresponding to the cross-sections given in Fig. 1(a) and Fig. 1(b). The above suggests that when cracking occurs, it will affect, first, the structures corresponding to the geometry of Fig. 1(c); however if the crack occurs in a structure corresponding to the geometries of Fig. 1(a) and Fig. 1(b), one should expect to have a shear failure of the lattice in a large neighbourhood of the defect.

https://doi.org/10.1017/S0956792599003654 Published online by Cambridge University Press

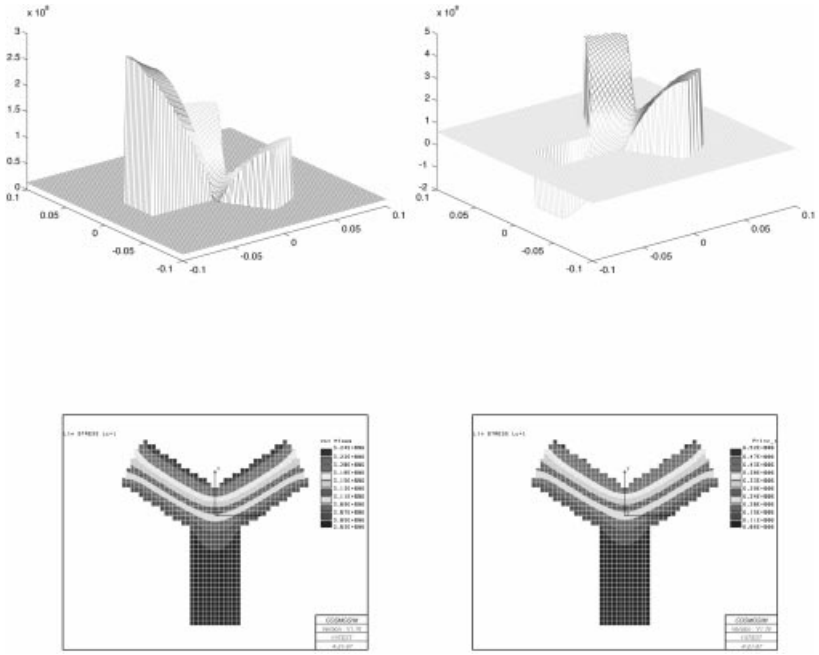

FIGURE 5. The cross-section (b); $z = 0.3l$. 3D graphs of the von Mises stress (top-left) and the greatest principal eigenvalue (top-right). 2D COSMOS/M contours of the the von Mises stress (bottom-left) and the greatest principal eigenvalue (bottom-right) for the field **U**. First numerical test.

5 Honeycomb structure under remote loading

In this section we present the homogenization procedure for thin-wall structures. The asymptotic approach gives us the expansion of the model displacement fields and, as a result, the asymptotic approximation of the effective moduli. It will be shown that the leading term of this expansion agrees with the known 'engineering approach' [14, 15]. However, we derive the 'junction boundary conditions' in a rigorous way, and obtain high order corrections for the effective elastic moduli. That enables us to evaluate the shear moduli of the thin-walled composites, unavailable in the general engineering literature.

5.1 Formal asymptotic approach

Consider a periodic structure, in other words the structure which can be obtained by a shift of an elementary cell $\mathscr{S}$ in two non-parallel directions. In 2D the elementary cell could be a parallelogram, square, rectangle or hexagon. One can reduce the problem formulated for the whole composite to the problem for a single cell only.

Let $\Xi^{(\varepsilon)}$ be a domain defined as a union of thin regions $\Pi_{\varepsilon}^{(n)} = \{(x_1^{(n)},\ x_2^{(n)}) : 0 < x_1^{(n)} < L,\ |x_2^{(n)}| < \varepsilon/2\}, 0 < \varepsilon \ll 1, n = 1,\ldots,N$ (where $x_1^{(n)},\ x_2^{(n)}$ are the local coordinates shown in Fig. 16) and junction area $\mathscr{O}^{(\varepsilon)}$; $\Xi^{(\varepsilon)}$ covers the whole elementary cell of the periodic structure excluding voids.

The junction region is specified in such a way, that $\mathscr{O} \subset [-C\varepsilon,\ C\varepsilon] \times [-D\varepsilon,\ D\varepsilon]$, where

https://doi.org/10.1017/S0956792599003654 Published online by Cambridge University Press

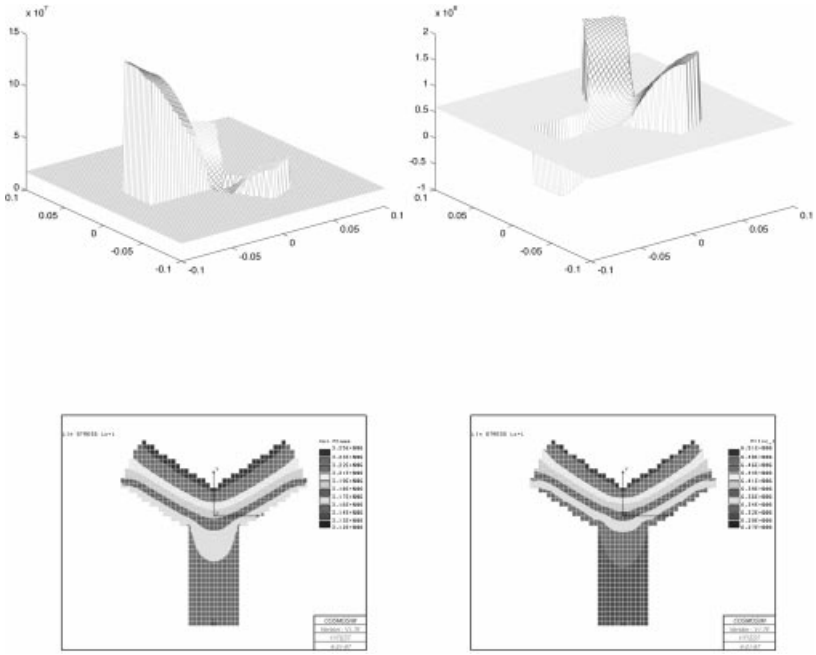

FIGURE 6. The cross-section (b); $z = 0.7l$. 3D graphs of the von Mises stress (top-left) and the greatest principal eigenvalue (top-right). 2D COSMOS/M contours of the the von Mises stress (bottom-left) and the greatest principal eigenvalue (bottom-right) for the field $\mathbf{U}$. First numerical test.

C and D are some constants. The junction region characterized the area where the bridges join each other ($\mathcal{O} \subset \cup_{n,k}(\Pi^{(n)} \cap \Pi^{(k)})$).

The boundary of the thin-wall structure inside the elementary cell $\mathcal{S}$ is split into two parts. First, $\partial\Xi_1^{(\varepsilon)}$ is defined as the lateral part of the boundary $\partial\Xi^{(\varepsilon)}$, $\partial\Xi^{(\varepsilon)} \cap \partial\mathcal{S} = \emptyset$. The remaining part is $\partial\Xi_2^{(\varepsilon)} = \partial\Xi^{(\varepsilon)} \setminus \partial\Xi_1^{(\varepsilon)}$ associated with the border of the periodic cell.

The elasticity problem in $\Xi^{(\varepsilon)}$ can be formulated in the following form. On the lateral boundary of the bridges and junction, we impose free traction boundary conditions and on the edges of the bridges the displacement conditions are specified[1]:

$$\mu\Delta\mathbf{U}(\mathbf{x}) + (\lambda + \mu)\nabla\nabla \cdot \mathbf{U}(\mathbf{x}) = \mathbf{0}, \quad \mathbf{x} \in \Xi^{(\varepsilon)},$$

$$\boldsymbol{\sigma}^{(n)}(\mathbf{U}, \mathbf{x}) = \mathbf{0}, \quad \mathbf{x} \in \partial\Xi_1^{(\varepsilon)},$$

$$\mathbf{U}(\mathbf{x}) = \mathbf{U}^*(\mathbf{x}), \quad \mathbf{x} \in \partial\Xi_2^{(\varepsilon)}, \tag{47}$$

where $\mathbf{U}^*(\mathbf{x})$ is the trace of the test field.

As we shall see, in the limit case, when the thickness of the bridges tends to zero (or has the order $O(\varepsilon)$, where ε is a small parameter), the solution of the system (47) can be represented as a linear combination of solutions of model problems corresponding to each bridge plus and the solution of a model problem in the junction region. By the

[1] The values of these displacements are defined by the compound problem, including the nearby periodic cells.

https://doi.org/10.1017/S0956792599003654 Published online by Cambridge University Press

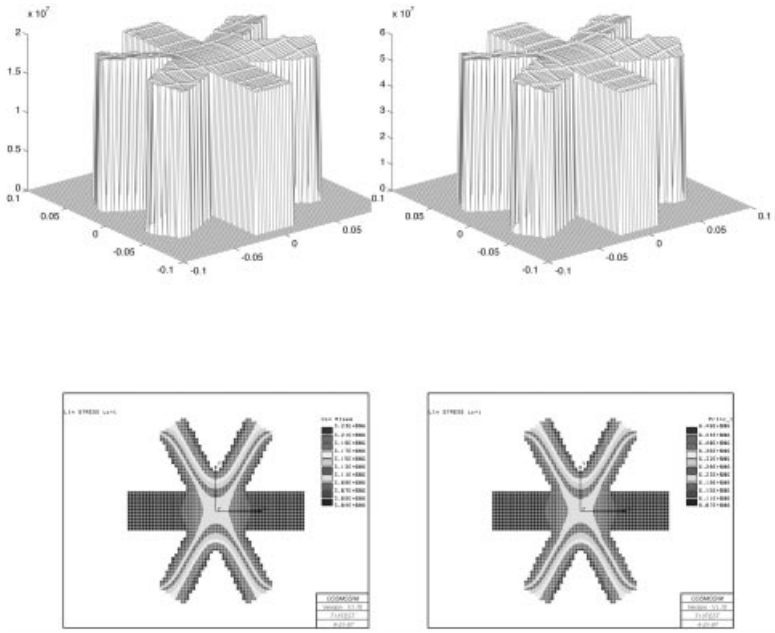

FIGURE 7. The cross-section (c); $z = 0.3l$. 3D graph of the von Mises stress (top-left) and the greatest principal eigenvalue (top-right). 2D COSMOS/M contours of the the von Mises stress (bottom-left) and the greatest principal eigenvalue (bottom-right) for the field **U**. First numerical test.

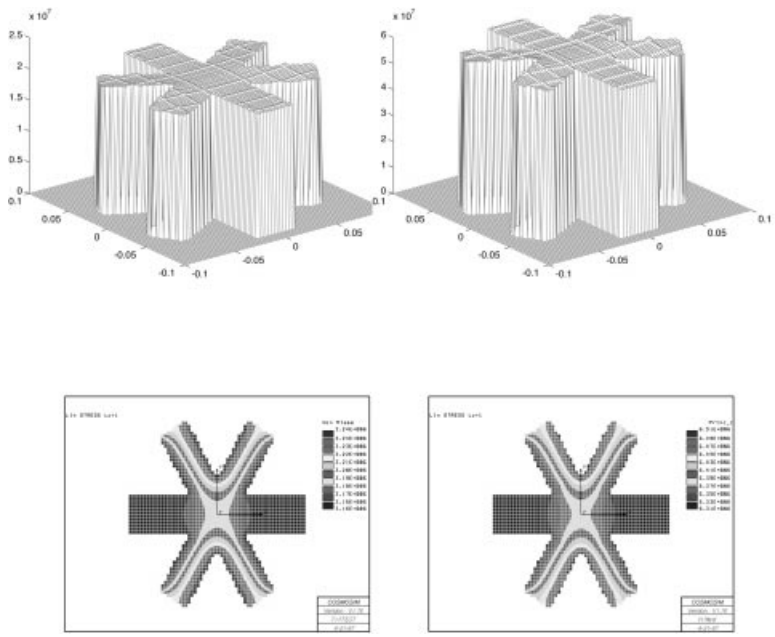

FIGURE 8. The cross-section (c); $z = 0.7l$. 3D graph of the von Mises stress (top-left) and the greatest principal eigenvalue (top-right). 2D COSMOS/M contours of the the von Mises stress (bottom-left) and the greatest principal eigenvalue (bottom-right) for the field **U**. First numerical test.

https://doi.org/10.1017/S0956792599003654 Published online by Cambridge University Press

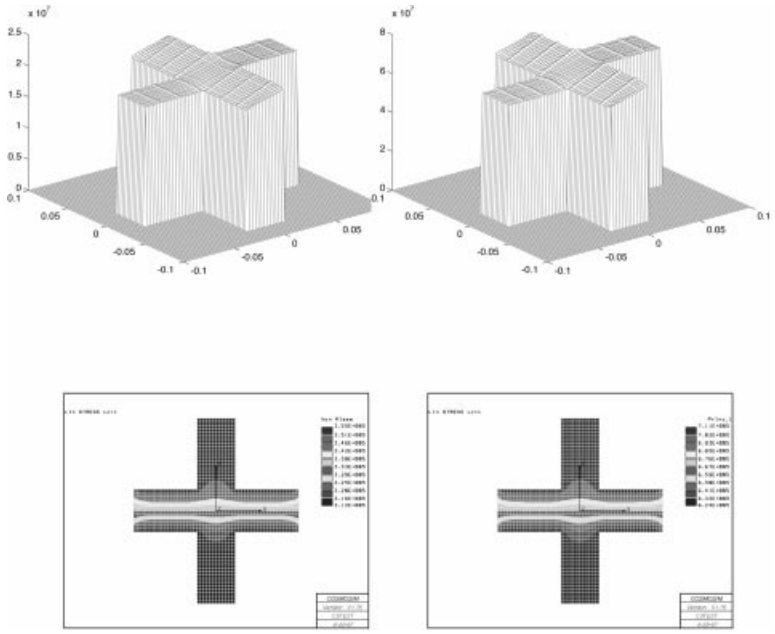

FIGURE 9. The cross-section (a); $z = 0.3l$. 3D graphs of the von Mises stress (top-left) and the greatest principal eigenvalue (top-right). 2D COSMOS/M contours of the the von Mises stress (bottom-left) and the greatest principal eigenvalue (bottom-right) for the field $\mathbf{U}$. Second numerical test.

asymptotic technique the displacement field for each thin bridge $\Pi^{(n)}$ can be represented as a series (see Bakhvalov & Panasenko [16] and Appendix A.4 for detailed analysis):

$$\mathbf{U}^{(n)}(\mathbf{x}) \sim \sum_{i=0}^{\infty} \varepsilon^i \left[\sum_{k=0}^{2} \varepsilon^k \boldsymbol{\mathcal{U}}_{i,k}^{(n)} + \sum_{k=0}^{4} \varepsilon^k \boldsymbol{\mathcal{V}}_{i,k}^{(n)} \right], \quad \mathbf{x} \in \Pi^{(n)}. \tag{48}$$

If the lateral surface of the bridge is free of traction (which is true for a honeycomb with voids) the leading term of this expansion has the following vector polynomial form (it is assumed that each thin bridge has a constant thickness):

$$\mathbf{U}^{(n)} \sim \boldsymbol{\mathcal{U}}_{0,0}^{(n)} + \boldsymbol{\mathcal{V}}_{0,0}^{(n)}, \quad \boldsymbol{\mathcal{U}}_{0,0}^{(n)} = \begin{pmatrix} u_0^{(n)} \\ 0 \end{pmatrix} = \begin{pmatrix} A^{(n)} x^{(n)} + B^{(n)} \\ 0 \end{pmatrix},$$

$$\boldsymbol{\mathcal{V}}_{0,0}^{(n)} = \begin{pmatrix} 0 \\ v_0^{(n)} \end{pmatrix} = \begin{pmatrix} 0 \\ C^{(n)}(x^{(n)})^3 + D^{(n)}(x^{(n)})^2 + E^{(n)} x^{(n)} + F^{(n)} \end{pmatrix}, \tag{49}$$

where $x^{(n)}$ is the local coordinate along the bridge and the coefficients $A^{(n)}, B^{(n)}, C^{(n)}, D^{(n)}$, $E^{(n)}, F^{(n)}$ are defined from the boundary conditions on the edges of the bridges and the 'junction boundary condition'.

Our intention is to derive the 'junction boundary condition' from the analysis of the boundary layer near the junction point.

The smooth cut-off function is defined for each thin region and it is equal to 0 in the

https://doi.org/10.1017/S0956792599003654 Published online by Cambridge University Press

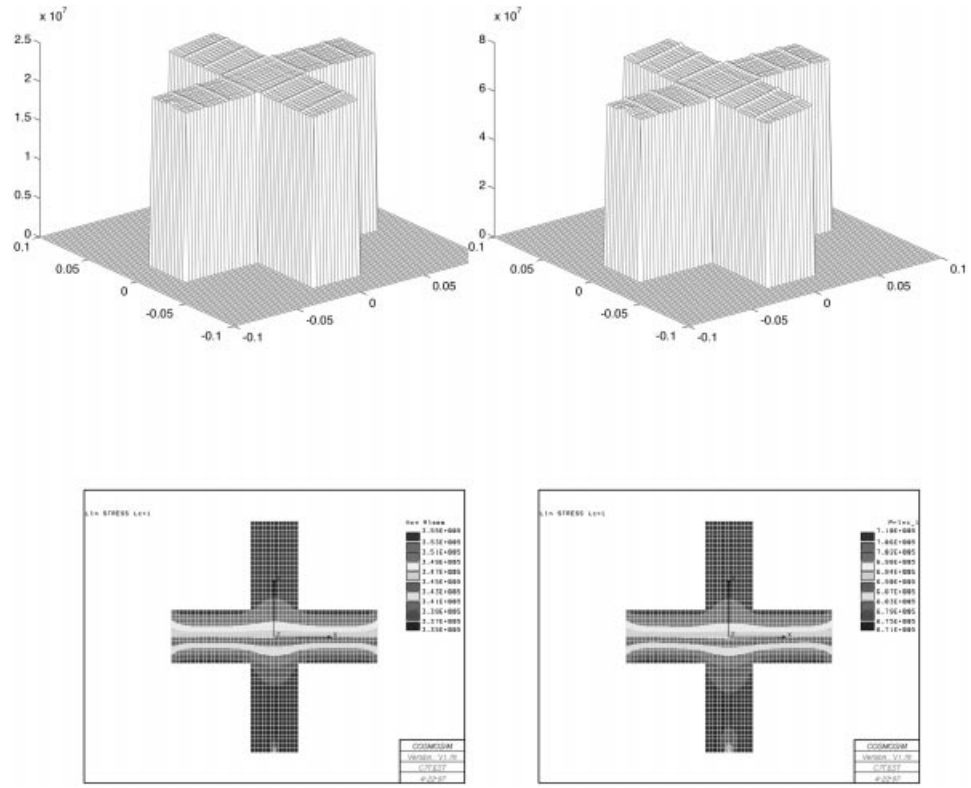

FIGURE 10. The cross-section (a); $z = 0.7l$. 3D graphs of the von Mises stress (top-left) and the greatest principal eigenvalue (top-right). 2D COSMOS/M contours of the the von Mises stress (bottom-left) and the greatest principal eigenvalue (bottom-right) for the field **U**. Second numerical test.

junction area and 1 in the thin bridge (far away from the junction point):

$$\chi(X^{(n)}) = 1, \quad \text{for } X^{(n)} > 1 \quad \text{and} \quad \chi(X^{(n)}) = 0, \quad \text{for } X^{(n)} < 1/2.$$

Here $\mathbf{X}^{(n)} = \mathbf{x}^{(n)}/\varepsilon$ are the 'fast' local variables.

Under such notation the solution $\mathbf{u}(\mathbf{x})$ of the equilibrium equation (47) can be represented in the form:

$$\mathbf{U}(\mathbf{x}) = \sum_{n=1}^{N} \chi(\mathbf{X}^{(n)})\, \mathbf{U}^{(n)}(\mathbf{x}^{(n)}) + \mathscr{W}\hat{}(\mathbf{X}), \tag{50}$$

where $\mathbf{U}^{(n)}(\mathbf{x})$ is the asymptotic expansion of the solution in the thin bridge (48), $\chi(\mathbf{X}^{(n)})$ is a cut-off function, $\mathscr{W}\hat{}(\mathbf{X})$ is the boundary layer solution (it decays exponentially), which admits the asymptotic representation

$$\mathscr{W}\hat{}(\mathbf{X}) = \sum_{i=0}^{\infty} \varepsilon^i\, \mathscr{W}\hat{}^{(i)}(\mathbf{X}). \tag{51}$$

In the formulae above the 'fast' global variables $\mathbf{X}$ are introduced like $\mathbf{X} = \mathbf{x}/\varepsilon$.

Substituting (50) in the governing equations and collecting the coefficients near like powers of ε we obtain the set of boundary value problems in the scaled region $\Xi^{(\varepsilon)}$.

https://doi.org/10.1017/S0956792599003654 Published online by Cambridge University Press

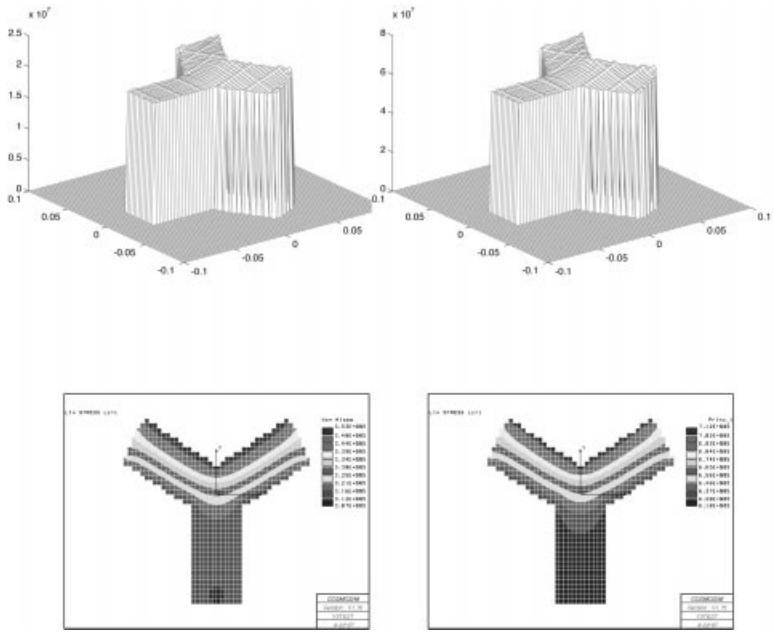

FIGURE 11. The cross-section (b); $z = 0.3l$. 3D graphs of the von Mises stress (top-left) and the greatest principal eigenvalue (top-right). 2D COSMOS/M contours of the the von Mises stress (bottom-left) and the greatest principal eigenvalue (bottom-right) for the field **U**. Second numerical test.

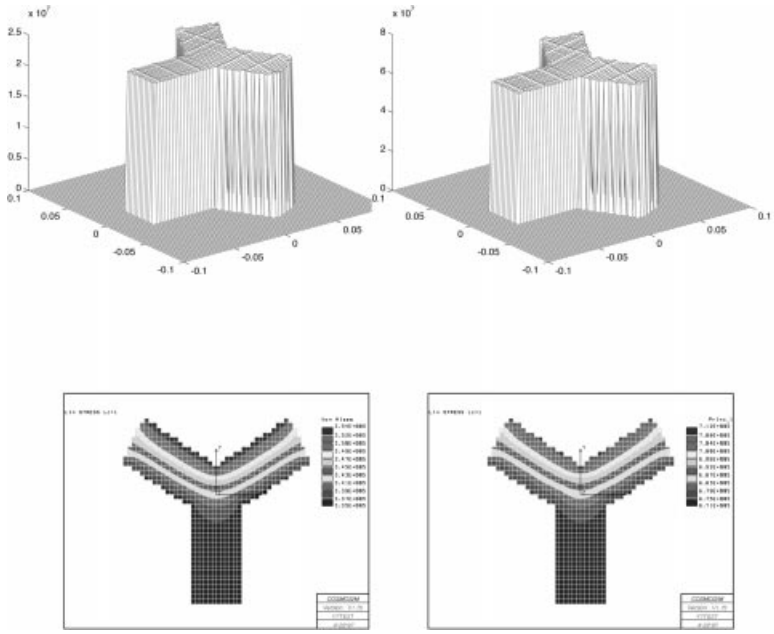

FIGURE 12. The cross-section (b); $z = 0.7l$. 3D graphs of the von Mises stress (top-left) and the greatest principal eigenvalue (top-right). 2D COSMOS/M contours of the the von Mises stress (bottom-left) and the greatest principal eigenvalue (bottom-right) for the field **U**. Second numerical test.

https://doi.org/10.1017/S0956792599003654 Published online by Cambridge University Press

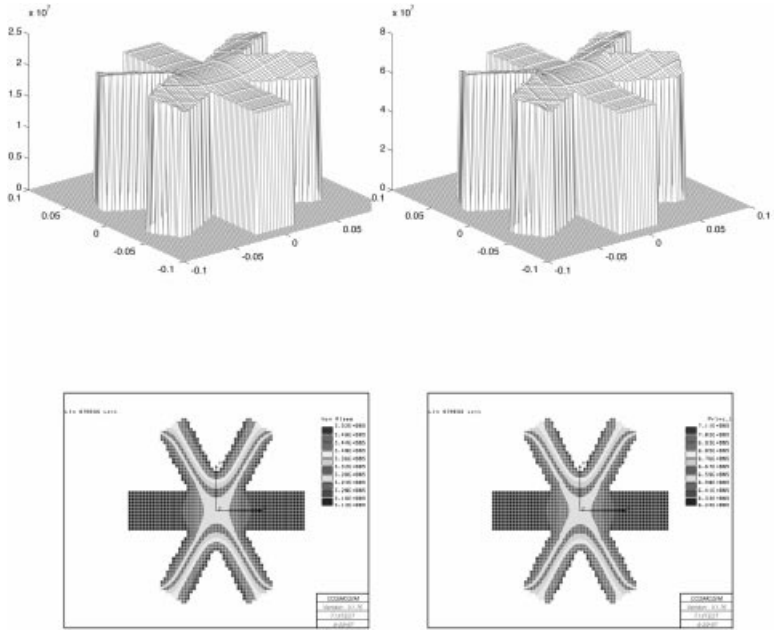

FIGURE 13. The cross-section (c); $z = 0.3l$. 3D graph of the von Mises stress (top-left) and the greatest principal eigenvalue (top-right). 2D COSMOS/M contours of the the von Mises stress (bottom-left) and the greatest principal eigenvalue (bottom-right) for the field **U**. Second numerical test.

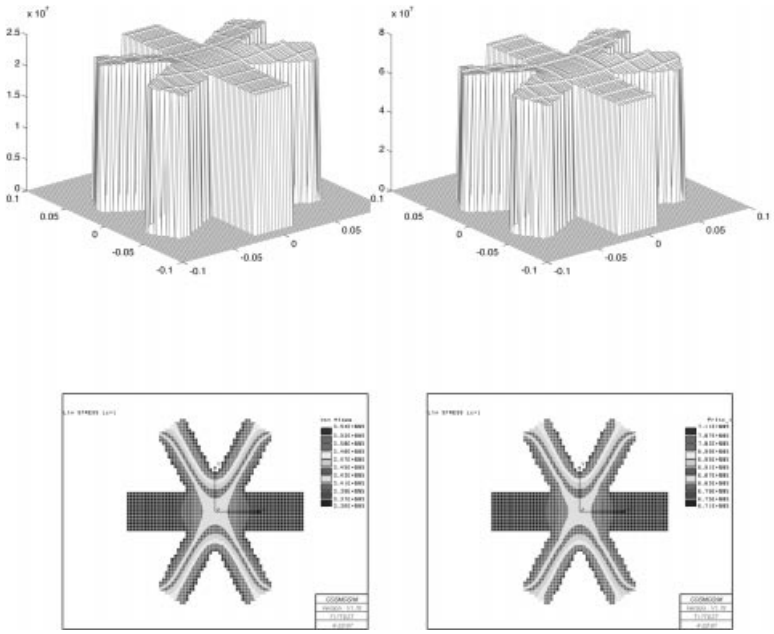

FIGURE 14. The cross-section (c); $z = 0.7l$. 3D graph of the von Mises stress (top-left) and the greatest principal eigenvalue (top-right). 2D COSMOS/M contours of the the von Mises stress (bottom-left) and the greatest principal eigenvalue (bottom-right) for the field **U**. Second numerical test.

https://doi.org/10.1017/S0956792599003654 Published online by Cambridge University Press

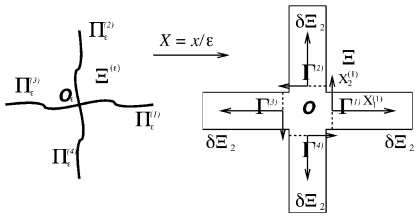

FIGURE 15. Deformation of the junction region in the honeycomb structure.

5.1.1 *First boundary layer*

The first boundary layer compensates for the discrepancy left by the leading term of the asymptotic expansion in $\cup_{n=1}^{N} \Pi_\varepsilon^{(n)}$. As a result, the first boundary layer problem is the inhomogeneous problem, where body forces and surface traction are the functions of $u_0^{(n)}, v_0^{(n)}$ only. The condition of exponential decay of the boundary layer at infinity is imposed:

$$\begin{aligned} \mathscr{L}(\boldsymbol{\mathscr{W}}^{(0)}, \mathbf{X}) + \mathscr{F}_0(\mathbf{X}) &= \mathbf{0}, \quad \mathbf{X} \in \Xi, \\ \boldsymbol{\sigma}^{(n)}(\boldsymbol{\mathscr{W}}^{(0)}, \mathbf{X}) + \mathscr{P}_0(\mathbf{X}) &= \mathbf{0}, \quad \mathbf{X} \in \partial\Xi_1, \\ \boldsymbol{\mathscr{W}}^{(0)} &\to \mathbf{0}, \quad \|\mathbf{x}\| \to \infty, \end{aligned} \tag{52}$$

where the body forces and surface tractions are specified as

$$\mathscr{F}_0(\mathbf{X}) = \sum_{m=1}^{N} \chi''(X_1^{(m)}) \begin{pmatrix} (2\mu+\lambda)\, u_0^{(m)}(0) \\ \mu v_0^{(m)}(0) \end{pmatrix}, \quad \mathscr{P}_0(\mathbf{X}) = \sum_{m=1}^{N} \chi'(X_1^{(m)}) \begin{pmatrix} \mu v_0^{(m)}(0) \\ \lambda u_0^{(m)}(0) \end{pmatrix}, \tag{53}$$

and Ξ and $\partial\Xi_1$ are the domain $\Xi^{(\varepsilon)}$ and its boundary enlarged in ε^{-2} times.

The vector-valued functions (53) satisfy the orthogonality conditions

$$\int_{\Xi} \boldsymbol{\mathscr{F}}^{(0)}\, d\mathbf{X} - \int_{\partial\Xi} \boldsymbol{\mathscr{P}}^{(0)}\, ds = \mathbf{0}, \tag{54}$$

$$\int_{\Xi} \mathbf{X} \times \boldsymbol{\mathscr{F}}^{(0)}\, d\mathbf{X} - \int_{\partial\Xi} \mathbf{X} \times \boldsymbol{\mathscr{P}}^{(0)}\, ds = \mathbf{0}. \tag{55}$$

We can reduce this boundary layer problem to the problem in a finite domain. It corresponds to the fact that the body forces and the surface tractions located in the region of enlarged thin bridges (where $\chi'(X^{(n)})$ and $\chi''(X^{(n)})$ are not equal to 0). Thus, the junction area is described by the homogeneous Navier system with zero traction on the lateral surface. In the region $\Xi \setminus \mathscr{O}$ the solution of the problem (52) admits the following expansion:

$$\boldsymbol{\mathscr{W}}^{(0)} = \begin{cases} \begin{pmatrix} u_0^{(n)}(0) \\ v_0^{(n)}(0) \end{pmatrix} (1 - \chi(X_1^{(n)})), & \mathbf{X}^{(n)} \in \Xi \setminus \mathscr{O} \\ \boldsymbol{\mathscr{W}}^{(0,1)}, & \mathbf{X} \in \mathscr{O} \end{cases} \tag{56}$$

where $\mathbf{X}^{(n)}$ are the local coordinates associated with the bridge, and the field $\boldsymbol{\mathscr{W}}^{(0,1)}$ satisfies

https://doi.org/10.1017/S0956792599003654 Published online by Cambridge University Press

the following problem in $\mathcal{O}$ (enlarged junction region, see Fig. 15):

$$\begin{gathered}\mathscr{L}(\boldsymbol{\mathcal{W}}^{(0,1)}, \mathbf{X}) = \mathbf{0}, \quad \mathbf{X} \in \mathcal{O},\\ \boldsymbol{\sigma}^{(n)}(\boldsymbol{\mathcal{W}}^{(0,1)}, \mathbf{X}) = \mathbf{0}, \quad \mathbf{X} \in \partial\Xi_1 \setminus \Gamma^{(i)},\\ \Gamma^{(1)}: \quad \boldsymbol{\mathcal{W}}^{(0,1)} = \begin{pmatrix} u_0^{(1)}(0) \\ v_0^{(1)}(0) \end{pmatrix} \qquad \Gamma^{(2)}: \quad \boldsymbol{\mathcal{W}}^{(0,1)} = \begin{pmatrix} -v_0^{(2)}(0) \\ u_0^{(2)}(0) \end{pmatrix},\\ \Gamma^{(3)}: \quad \boldsymbol{\mathcal{W}}^{(0,1)} = \begin{pmatrix} -u_0^{(3)}(0) \\ -v_0^{(3)}(0) \end{pmatrix} \qquad \Gamma^{(4)}: \quad \boldsymbol{\mathcal{W}}^{(0,1)} = \begin{pmatrix} v_0^{(4)}(0) \\ -u_0^{(4)}(0) \end{pmatrix},\end{gathered} \tag{57}$$

where $\Gamma^{(i)}$ are parts of the boundary shown in Fig. 15.

Now our intention is to find the solution of this system and satisfy the continuity of displacement and traction on $\Gamma^{(1)}$, $\Gamma^{(2)}$, $\Gamma^{(3)}$, $\Gamma^{(4)}$. Such conditions arise from the matching with the solution in thin bridges (56). Note that solution (56) produces zero tractions on the boundary $\Gamma^{(n)}$. It follows from the fact that $\chi'(X_1^{(n)}) = 0$ when $\mathbf{X}^{(n)} \in \Gamma^{(n)}$. Therefore, on all parts of the boundary $\mathcal{O}$ we have zero traction, and the solution must be represented as the vector with constant components (it corresponds to the rigid translation of the region $\mathcal{O}$).

We can find such kind of solution (with 'constant' displacement field inside $\mathcal{O}$) if and only if the following conditions hold:

$$\begin{aligned} u_0^{(1)}(0) &= -v_0^{(2)}(0) = -u_0^{(3)}(0) = v_0^{(4)}(0),\\ v_0^{(1)}(0) &= u_0^{(2)}(0) = -v_0^{(3)}(0) = -u_0^{(4)}(0). \end{aligned} \tag{58}$$

Under such conditions (58) the field $\boldsymbol{\mathcal{W}}^{(0,1)}$ has zero energy and the continuity of tractions on $\Gamma^{(n)}$ is satisfied.

5.1.2 *Second boundary layer*

Applying a similar procedure for the construction of the boundary layer for the next asymptotic term of (51), we obtain the following boundary value problem for the field $\boldsymbol{\mathcal{W}}^{(1)}$:

$$\begin{aligned} \mathscr{L}(\boldsymbol{\mathcal{W}}^{(1)}, \mathbf{X}) + \boldsymbol{\mathcal{F}}^{(1)}(\mathbf{X}) &= \mathbf{0}, \quad \mathbf{X} \in \Xi,\\ \boldsymbol{\sigma}^{(n)}(\boldsymbol{\mathcal{W}}^{(1)}, \mathbf{X}) + \boldsymbol{\mathcal{P}}^{(1)}(\mathbf{X}) &= \mathbf{0}, \quad \mathbf{X} \in \partial\Xi,\\ \boldsymbol{\mathcal{W}}^{(1)} &\to \mathbf{0}, \quad \|\mathbf{x}\| \to \infty, \end{aligned} \tag{59}$$

where

$$\begin{aligned} \boldsymbol{\mathcal{F}}^{(1)}(\mathbf{X}) = \sum_{m=1}^{N} \Bigg\{ \chi''(X_1^{(m)}) \begin{pmatrix} (2\mu+\lambda)\,(X_1^{(m)}\,\partial_x u_0^{(m)}(0) - X_2^{(m)}\,\partial_x v_0^{(m)}(0) + u_1^{(m)}(0)) \\ \mu\left(-\dfrac{\lambda X_2^{(m)}}{\lambda+2\mu}\partial_x u_0^{(m)}(0) + X_1^{(m)}\,\partial_x v_0^{(m)}(0) + v_1^{(m)}(0)\right) \end{pmatrix}\\ + \chi'(X_1^{(m)}) \begin{pmatrix} \left\{2(2\mu+\lambda) - \dfrac{\lambda(\lambda+\mu)}{\lambda+2\mu}\right\}\partial_x u_0^{(m)}(0) \\ (\mu+\lambda)\,\partial_x v_0^{(m)}(0) \end{pmatrix} \Bigg\}, \end{aligned}$$

$$\boldsymbol{\mathcal{P}}^{(1)}(\mathbf{X}) = \sum_{m=1}^{N} \chi'(X_1^{(m)}) \begin{pmatrix} \mu\left(-\dfrac{\lambda X_2^{(m)}}{\lambda+2\mu}\,\partial_x u_0^{(m)}(0) + X_1^{(m)}\,\partial_x v_0^{(m)}(0) + v_1^{(m)}(0)\right) \\ \lambda(X_1^{(m)}\,\partial_x u_0^{(m)}(0) - X_2^{(m)}\,\partial_x v_0^{(m)}(0) + u_1^{(m)}(0)) \end{pmatrix}.$$

https://doi.org/10.1017/S0956792599003654 Published online by Cambridge University Press

This problem admits a solution which decays at infinity, provided the following orthogonality conditions for (59) hold:

$$\int_{\Xi} \mathscr{F}_1^{(j)}\, d\mathbf{X} - \int_{\partial\Xi} \mathscr{P}_1^{(j)}\, ds = 0, \quad j = 1, 2, \tag{60}$$

$$\int_{\Xi} X_1 \mathscr{F}_2^{(1)} - X_2 \mathscr{F}_1^{(1)} d\mathbf{X} - \int_{\partial\Xi} X_1 \mathscr{P}_2^{(1)} - X_2 \mathscr{P}_1^{(1)} ds = 0. \tag{61}$$

The conditions (60) can be represented in the following simplified form:

$$\partial_x u^{(1)}(0) - \partial_x u^{(3)}(0) = 0, \quad \partial_x u^{(2)}(0) - \partial_x u^{(4)}(0) = 0, \tag{62}$$

The condition (61) is satisfied identically.

Following the procedure employed for the first boundary layer we reduce our problem in an infinite domain to the problem in a finite domain. We use the following properties of the system (59): inside the region $\mathscr{O}$ it is homogeneous, and effects of the action of the cut-off function can be transformed into Dirichlet boundary conditions imposed on $\Gamma^{(n)}$. As before, the field $\boldsymbol{\mathscr{W}}^{\gamma(1)}$ is sought in the form

$$\boldsymbol{\mathscr{W}}^{\gamma(1)} = \begin{cases} \begin{pmatrix} X_1^{(n)}\, \partial_x u_0^{(n)}(0) + u_1^{(n)}(0) - X_2^{(n)}\, \partial_x v_0^{(n)}(0) \\ -\dfrac{\lambda X_2^{(n)}}{\lambda + 2\mu}\, \partial_x u_0^{(n)}(0) + v_1^{(n)}(0) + X_1^{(n)}\, \partial_x v_0^{(n)}(0) \end{pmatrix} (1 - \chi(X_1^{(n)})), & \mathbf{X}^{(n)} \in \Xi \setminus \mathscr{O} \\ \boldsymbol{\mathscr{W}}^{\gamma(1,1)}, & \mathbf{X} \in \mathscr{O} \end{cases} \tag{63}$$

where $\boldsymbol{\mathscr{W}}^{\gamma(1,1)}(\mathbf{X})$ satisfies the following system:

$$\begin{aligned} \mathscr{L}(\boldsymbol{\mathscr{W}}^{\gamma(1,1)}, \mathbf{X}) &= \mathbf{0}, \quad \mathbf{X} \in \mathscr{O}, \\ \boldsymbol{\sigma}^{(n)}(\boldsymbol{\mathscr{W}}^{\gamma(1,1)}, \mathbf{X}) &= \mathbf{0}, \quad \mathbf{X} \in \partial\Xi_1 \setminus \Gamma^{(i)}. \end{aligned} \tag{64}$$

Boundary conditions on $\Gamma^{(i)}$ are as follows:

$$\Gamma^{(1)}: \quad \boldsymbol{\mathscr{W}}^{\gamma(1,1)} = \begin{pmatrix} X_1\, \partial_x u_0^{(1)}(0) + u_1^{(1)}(0) \\ -\dfrac{\lambda X_2}{\lambda + 2\mu}\, \partial u_0^{(1)}(0) + v_1^{(1)}(0) \end{pmatrix} + \begin{pmatrix} -X_2\, \partial_x v_0^{(1)}(0) \\ X_1\, \partial_x v_0^{(1)}(0) \end{pmatrix},$$

$$\Gamma^{(2)}: \quad \boldsymbol{\mathscr{W}}^{\gamma(1,1)} = \begin{pmatrix} -\dfrac{\lambda X_1}{\lambda + 2\mu}\, \partial u_0^{(2)}(0) - v_1^{(2)}(0) \\ X_2\, \partial_x u_0^{(2)}(0) + u_1^{(2)}(0) \end{pmatrix} + \begin{pmatrix} -X_2\, \partial_x v_0^{(2)}(0) \\ X_1\, \partial_x v_0^{(2)}(0) \end{pmatrix},$$

$$\Gamma^{(3)}: \quad \boldsymbol{\mathscr{W}}^{\gamma(1,1)} = \begin{pmatrix} X_1\, \partial_x u_0^{(3)}(0) - u_1^{(3)}(0) \\ -\dfrac{\lambda X_2}{\lambda + 2\mu}\, \partial u_0^{(3)}(0) - v_1^{(3)}(0) \end{pmatrix} + \begin{pmatrix} -X_2\, \partial_x v_0^{(3)}(0) \\ X_1\, \partial_x v_0^{(3)}(0) \end{pmatrix},$$

$$\Gamma^{(4)}: \quad \boldsymbol{\mathscr{W}}^{\gamma(1,1)} = \begin{pmatrix} -\dfrac{\lambda X_1}{\lambda + 2\mu}\, \partial u_0^{(4)}(0) + v_1^{(4)}(0) \\ X_2\, \partial_x u_0^{(4)}(0) - u_1^{(4)}(0) \end{pmatrix} + \begin{pmatrix} -X_2\, \partial_x v_0^{(4)}(0) \\ X_1\, \partial_x v_0^{(4)}(0), \end{pmatrix}$$

where X_1, X_2 are the global 'fast' coordinates associated with the junction region.

https://doi.org/10.1017/S0956792599003654 Published online by Cambridge University Press

The traction on the boundary $\Gamma^{(n)}$ can be evaluated as

$$\sigma^{(n)}(\mathscr{W}^{(1)};\ \mathbf{X}^{(n)}) = \begin{pmatrix} \dfrac{4\mu(\lambda+\mu)}{\lambda+2\mu}\,\partial_x u_0^{(n)}(0) \\ 0 \end{pmatrix}.$$

The energy accumulated in the junction region is given by

$$\begin{aligned}\Delta\mathscr{E}_{\mathscr{O}} &= -\int_{\partial\Xi\cup\Gamma^{(n)}} \sigma^{(n)}(\mathscr{W}^{(1,1)};\ \mathbf{X}^{(n)})\mathscr{W}^{(1,1)}(\mathbf{X}^{(n)})\,ds \\ &= \sum_{n=1}^{N} \frac{4\mu(\lambda+\mu)}{\lambda+2\mu}\,\partial_x u_0^{(n)}(0)\big[X_1^{(n)}\,\partial_x u_0^{(n)}(0) + u_1^{(n)}(0)\big],\end{aligned}$$

where $X_1^{(n)}$ is on the boundary $\Gamma^{(n)}$; the terms $\partial_x v_0^{(n)}(0)$ are not present in the expression for the energy integral.

'Rotation' conditions for the transversal displacement are imposed in the form

$$\partial_x v_0^{(1)}(0) = \partial_x v_0^{(2)}(0) = \partial_x v_0^{(3)}(0) = \partial_x v_0^{(4)}(0). \tag{65}$$

The condition (65) has a simple physical meaning. It corresponds to the fact that the *junction behaves like a rigid solid* when we restrict ourselves to the leading term of the displacement field. This property holds for a junction of any shape including three-beam and six-beam junctions.

If we consider next junction layer problems we get additional restrictions for the coefficients A, B, C, D, E, F (as the solvability conditions of corresponding equations). Namely, from the *third junction layer*:

$$\sum_{m=1}^{4} \partial_x^2 v_0^{(m)}(0) = 0, \tag{66}$$

and from the *fourth junction layer*:

$$\partial_x^3 v^{(1)}(0) - \partial_x^3 v^{(3)}(0) = 0, \quad \partial_x^3 v^{(2)}(0) - \partial_x^3 v^{(4)}(0) = 0. \tag{67}$$

Due to the solvability conditions (62), (66), (67) and continuity conditions (58), (65) the set of coefficients A, B, C, D, E, F is uniquely defined, and the leading term of the asymptotic approximations of the displacement field is obtained in closed form.

5.2 The leading order approximation for the effective moduli

It is known that the effective elastic moduli can be calculated as the energy of some special fields in the unit periodic cell (see Bakhvalov & Panasonko [16] and Appendix A.3 for details):

$$\mathscr{H}_{mk} = \frac{1}{mes_2\,\mathscr{S}} \int_{\Xi} \boldsymbol{\sigma}(\mathbf{U}^{(m)};\ \mathbf{x}) : \boldsymbol{\varepsilon}(\mathbf{U}^{(k)};\ \mathbf{x})\,d\mathbf{x}, \tag{68}$$

where $\boldsymbol{\sigma}$ and $\boldsymbol{\varepsilon}$ are stress and strain tensors, $\mathscr{S}$ is the elementary cell of the periodic structure (see Fig. 19). The model fields $\mathbf{U}^{(n)}$, $\mathbf{U}^{(k)}$ describe the displacements in the elementary cell when the whole composite is loaded by the test fields. Namely, $\varepsilon_{11} = 1$ for $n = 1$; $\varepsilon_{22} = 1$ for $n = 2$; $\varepsilon_{12} = 1$ for $n = 3$ (all other components of the strain tensor are supposed to be zero).

https://doi.org/10.1017/S0956792599003654 Published online by Cambridge University Press

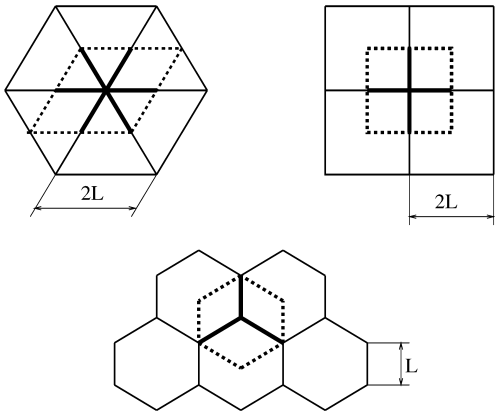

FIGURE 16. Three types of thin-walled structures.

The problem of evaluation of the effective moduli for honeycomb structures has been treated by Torquato *et al.* [15]. The authors used the approach based on the Hashin–Strikhman estimates for the effective characteristics of the composite structures. Such kind of treatment yields the approximations for the bulk and Young's moduli.

Our method of calculation is based on the asymptotic approach, and the estimates of the elastic energy give the total effective moduli matrix and allow one to take into account the high order terms. Also this approach works for composites where the thickness of 'thin bridges' is non-constant.

Now we can evaluate the energy of a single bridge assuming that the leading term of the asymptotic expansion (49) is known. In comparison with the case of the total asymptotic expansion, there is an additional simplification: the lateral surface of the bridge is free of tractions. It means that the first ansatz of the asymptotic expansion (see Appendix A.4 for full expansion) has the following form:

$$\mathscr{U}^{(n)} = \begin{pmatrix} u_0(x_1) \\ -\dfrac{\lambda}{\lambda+2\mu}\, x_2\, \partial_x\, u_0(x_1) \end{pmatrix},$$

$$\mathscr{V}^{(n)} = \begin{pmatrix} -x_2\, \partial_x\, v_0(x_1) + \dfrac{4\mu+3\lambda}{6(\lambda+2\mu)}\, x_2^3\, \partial^3_{xxx}\, v_0(x_1) + \varepsilon^2\, \dfrac{\mu+\lambda}{2(\lambda+2\mu)}\, x_2\, \partial^3_{xxx}\, v_0(x_1) \\ v_0(x_1) + \dfrac{\lambda}{\lambda+2\mu}\, \dfrac{x_2^2}{2}\, \partial^2_{xx}\, v_0(x_1) \end{pmatrix}, \quad (69)$$

where x_1, x_2 are the coordinates associated with the thin bridge.

The equations for the leading term components reduce to

$$\partial^2_{xx}\, u_0(x_1) = 0, \quad \partial^4_{xxxx}\, v_0(x_1) = 0,$$

with the Dirichlet boundary conditions prescribed on the edges.

One can calculate the components of the strain tensor associated with the above-

https://doi.org/10.1017/S0956792599003654 Published online by Cambridge University Press

Table 1. *For the honeycomb composites with constant thickness bridges the following relations hold.*

Type of honeycomb	N	Area $\mathscr{S}$	Area fraction f	Parameters for $S=1$	
Triangle[a]	6	$S=2\sqrt{3}L^2$	$f=\sqrt{3}\varepsilon L^{-1}$	$L=\frac{1}{\sqrt{2}\sqrt[4]{27}}$	$f=\frac{3\sqrt{2}\varepsilon}{\sqrt[4]{3}}$
Square[a]	4	$S=4L^2$	$f=\varepsilon L^{-1}$	$L=\frac{1}{2}$	$f=\frac{\varepsilon}{2}$
Hexagonal	3	$S=\frac{3}{2}\sqrt{3}L^2$	$f=\frac{2}{\sqrt{3}}\varepsilon L^{-1}$	$L=\frac{\sqrt{2}}{\sqrt[4]{27}}$	$f=\frac{\sqrt{6}\varepsilon}{\sqrt[4]{3}}$

[a] L is half the actual bridge length.

mentioned fields:

$$\varepsilon_{11}=\partial_x u_0(x_1)-x_2\,\partial^2_{xx}v_0(x_1),$$

$$\varepsilon_{22}=-\frac{\lambda}{\lambda+2\mu}\,\partial_x u_0(x_1)+\frac{\lambda}{\lambda+2\mu}\,x_2\,\partial^2_{xx}v_0(x_1),$$

$$\varepsilon_{12}=\frac{4\mu+3\lambda}{2(\lambda+2\mu)}\,x_2^2\,\partial^3_{xxx}v_0(x_1)+\frac{\lambda}{2(\lambda+2\mu)}\,x_2^2\,\partial^3_{xxx}v_0(x_1)-\varepsilon^2\frac{\lambda+\mu}{2(\lambda+2\mu)}\,\partial^3_{xxx}v_0(x_1).$$

Now we substitute the leading term of the solution (69) in the formula for the energy

$$\Delta\mathscr{E}_0=\int_0^L dx\int_{-\varepsilon/2}^{\varepsilon/2}\boldsymbol{\sigma}(\mathbf{U}^{(m)};\mathbf{x}):\boldsymbol{\varepsilon}(\mathbf{U}^{(k)};\mathbf{x})\,dy$$
$$=\frac{4\mu(\lambda+\mu)}{\lambda+2\mu}\int_0^L\left\{A^{(m)}A^{(k)}\,\varepsilon+\tfrac{1}{3}(3C^{(m)}x+D^{(m)})(3C^{(k)}x+D^{(k)})\,\varepsilon^3\right\}dx+O(\varepsilon^5),\quad(70)$$

where the quantities $A^{(k)}$, $C^{(k)}$ and $D^{(k)}$ are the same as in (49).

The energy of the elementary cell can be evaluated as the sum of energies of thin bridges. The junction area degenerates to the junction point, when the thickness of bridges tends to zero. The effective elastic moduli are specified as follows:[2]

$$\mathscr{H}_{mk}=\frac{1}{mes_2\,\mathscr{S}}\sum_{n=1}^{N}\Delta\mathscr{E}_0^{(n)}=\frac{4\mu(\lambda+\mu)}{mes_2\,\mathscr{S}(\lambda+2\mu)}\sum_{n=1}^{N}$$
$$\times\int_0^L\left\{A_n^{(m)}A_n^{(k)}\,\varepsilon+\tfrac{1}{3}(3C_n^{(m)}x+D_n^{(m)})(3C_n^{(k)}x+D_n^{(k)})\,\varepsilon^3\right\}dx+O(\varepsilon^5)\qquad(71)$$

where N is the number of bridges connected at the junction point ($N=3,4,6$), the index n corresponds to the number of the bridge, indices m,k correspond to the type of loading, L is the length of the bridge, $mes_2\,\mathscr{S}$ is the area of the elementary cell, and ε is the normalized thickness of the bridge.

Asymptotic formulae for effective elastic moduli of thin-bridges composites under the assumption of constant thickness of the bridges (f is the area fraction) are derived in the following form:

[2] The junction gives the effect for next (high order) terms of the approximation of the effective moduli, which is not considered in this section. At the same time we note that the second term of the asymptotic expansion of the effective moduli has the order $O(\varepsilon^2)$ and can be evaluated by solving the problem (64).

https://doi.org/10.1017/S0956792599003654 Published online by Cambridge University Press

Triangular honeycomb:

$$\mathscr{H} \simeq \frac{4\mu(\lambda+\mu)}{2\mu+\lambda}\begin{pmatrix} \frac{3}{8}f & \frac{1}{8}f & 0 \\ \frac{1}{8}f & \frac{3}{8}f & 0 \\ 0 & 0 & \frac{1}{4}f \end{pmatrix} \tag{72}$$

Square honeycomb:

$$\mathscr{H} \simeq \frac{4\mu(\lambda+\mu)}{2\mu+\lambda}\begin{pmatrix} \frac{1}{2}f & 0 & 0 \\ 0 & \frac{1}{2}f & 0 \\ 0 & 0 & \frac{1}{8}f^3 \end{pmatrix} \tag{73}$$

Hexagonal honeycomb:

$$\mathscr{H} \simeq \frac{4\mu(\lambda+\mu)}{2\mu+\lambda}\begin{pmatrix} \frac{1}{4}f+\frac{3}{8}f^3 & \frac{1}{4}f-\frac{3}{8}f^3 & 0 \\ \frac{1}{4}f-\frac{3}{8}f^3 & \frac{1}{4}f+\frac{3}{8}f^3 & 0 \\ 0 & 0 & \frac{3}{4}f^3 \end{pmatrix}. \tag{74}$$

Note, that the shear modulus ($\mathscr{H}_{33}$) has a different order in comparison with other effective moduli in the case of square and hexagonal honeycombs. It corresponds to the fact that these honeycombs have small resistance to the shear loading. Shear loading produces bending of bridges only.

Next, we evaluate the Young's modulus in the z-direction, the direction perpendicular to the cross-section of the honeycomb. Indeed, the calculations based on (68) give the following simple expression (one can compare this expression with the calculations of Young's modulus [17])

$$E_z = Ef = \frac{\mu(3\lambda+2\mu)}{\mu+\lambda}f. \tag{75}$$

The calculation of the effective thermal expansion coefficients is based on the formula

$$\Upsilon_{mk} = \frac{1}{mes_2\,\mathscr{S}}\int_{\Xi}\gamma(\mathbf{x})\nabla T^{(n)}\cdot\nabla T^{(k)}\,d\mathbf{x}, \tag{76}$$

where $\gamma(\mathbf{x})$ is the thermal expansion coefficient and $T^{(n)}, n=1,2$ are the temperature fields corresponding to the test fields x_1 and x_2 imposed on the composite structure.

The asymptotic procedure for the Laplace equation is even simpler than one presented earlier for the Lamé system, and the leading term of the temperature field inside each bridge can be obtained as the solution of the equation

$$\partial^2_{xx}\,T^{(n)} = 0, \quad 0 < x < L,$$

and hence

$$T^{(n)} = A^{(n)}\,x + B^{(n)}.$$

The appropriate Dirichlet data are specified at the end of the interval.

Then the thermal expansion matrix can be obtained as the sum of the Dirichlet integrals calculated for each bridge, multiplied by the thermal expansion coefficient of the bridge material:

$$\Upsilon_{mk} = \frac{\gamma}{mes_2\,\mathscr{S}}\sum_{n=1}^{N}\int_0^L A_n^{(m)}\,A_n^{(k)}\,\varepsilon\,dx + O(\varepsilon^2). \tag{77}$$

https://doi.org/10.1017/S0956792599003654 Published online by Cambridge University Press

For composite structures considered above the volume fraction of the material f is small and all bridges have a constant thickness ε. Finally, we derive that for all three types of composite structures the effective matrix of thermal expansion coefficients has the form

$$\Upsilon \simeq \gamma \begin{pmatrix} \frac{1}{2}f & 0 \\ 0 & \frac{1}{2}f \end{pmatrix}. \tag{78}$$

6 Conclusion

In this paper, we have presented an efficient semi-analytic approach for description of the stress state in thermo-elastic thin-walled composite structures encountered in catalytic combustor monoliths. The results include a numerical method based on the accurate asymptotic algorithm, and a set of 3D numerical tests carried out for analysis of the stress concentration at the junctions of the honeycomb structure. An accurate homogenization procedure was employed together with the asymptotic method to evaluate the effective elastic and thermal moduli of the composite structures.

The advantage of the asymptotic technique used in this work is that it enables one to solve the problem for the cases when the standard numerical techniques (like direct application of FEM) do not provide satisfactory accuracy. In addition, the homogenization analysis includes accurate asymptotic formulae even for the cases when the effective shear modulus of the monolith is small.

Further extension of this work is in analysis of thermal cracks propagating in a homogenized material with non-uniform distribution of temperature.

Acknowledgements

The work was supported by the U.K. Engineering and Physical Sciences Research Council (Grant No GR/K76634).

Appendix A.1 Definition of the functions $\boldsymbol{\phi}^{(k,j)}$

In this section we present the description of solutions of spectral problem associated with the Neumann boundary value problem for the Lamé system in an infinite cylinder $\Pi = \{(y_1, y_2) \in G,\ y_3 \in \mathbb{R}\}$, we adopt the notations

$$\mathbf{L}(\partial/\partial y_1, \partial/\partial y_2, \partial/\partial y_3), \quad \mathbf{T}(\partial/\partial y_1, \partial/\partial y_2, \partial/\partial y_3, \mathbf{n})$$

for the matrix differential operators of the Navier system and traction boundary conditions

$$\mathbf{L}(\xi_1, \xi_2, \xi_3) = \begin{pmatrix} (2\mu+\lambda)\xi_1^2 + \mu(\xi_2^2+\xi_3^2) & (\mu+\lambda)\xi_1\xi_2 & (\mu+\lambda)\xi_1\xi_3 \\ (\mu+\lambda)\xi_1\xi_2 & (2\mu+\lambda)\xi_2^2 + \mu(\xi_1^2+\xi_3^2) & (\mu+\lambda)\xi_2\xi_3 \\ (\mu+\lambda)\xi_3\xi_1 & (\mu+\lambda)\xi_3\xi_2 & (2\mu+\lambda)\xi_3^2 + \mu(\xi_1^2+\xi_2^2) \end{pmatrix},$$

$$\mathbf{T}(\xi_1, \xi_2, \xi_3) = n_1 \begin{pmatrix} (2\mu+\lambda)\xi_1 + \lambda\xi_2 & \lambda\xi_2 & \lambda\xi_3 \\ \mu\xi_2 & \mu\xi_1 & 0 \\ \mu\xi_3 & 0 & \mu\xi_1 \end{pmatrix} + n_2 \begin{pmatrix} \mu\xi_2 & \mu\xi_1 & 0 \\ \lambda\xi_1 & (2\mu+\lambda)\xi_2 + \lambda\xi_1 & \lambda\xi_3 \\ 0 & \mu\xi_3 & \mu\xi_2 \end{pmatrix};$$

where $\mathbf{n} = (n_1, n_2, 0)$ is the unit outward normal on the cylinder surface.

We seek the solution of

$$\mathbf{L}\left(\frac{\partial}{\partial y}\right)\boldsymbol{\Phi}^{(0)} = \mathbf{0} \ \text{ in } \Pi, \quad \mathbf{T}\left(\frac{\partial}{\partial y}, \mathbf{n}\right)\boldsymbol{\Phi}^{(0)} = \mathbf{0} \ \text{ on } \partial\Pi$$

in the form

$$\boldsymbol{\Phi}^{(0)} = e^{\Lambda y_3}\boldsymbol{\phi}^{(0)}(y_1, y_2),$$

where Λ and $\boldsymbol{\phi}^{(0)}$ are the eigenvalue and the eigenvector corresponding to the following spectral problem

$$L\left(\frac{\partial}{\partial \mathbf{y}'}, \Lambda\right)\boldsymbol{\phi}^{(0)}(\mathbf{y}') = \mathbf{0} \ \text{ in } G,$$

$$T\left(\frac{\partial}{\partial \mathbf{y}'}, \Lambda, \mathbf{n}\right)\boldsymbol{\phi}^{(0)}(\mathbf{y}') = \mathbf{0} \ \text{ on } \partial G,$$

where $\mathbf{y}' = (y_1, y_2)$.

In this work we are interested in the case when $\Lambda = 0$. We define the generalized eigenvectors $\boldsymbol{\phi}^{(k)}$, $k \geqslant 0$, to $\boldsymbol{\phi}^{(0)}$ and $\Lambda = 0$ in the following way:

$$\mathbf{L}\left(\frac{\partial}{\partial \mathbf{y}'}, 0\right)\boldsymbol{\phi}^{(k)}(\mathbf{y}') + \frac{\partial \mathbf{L}}{\partial \Lambda}\left(\frac{\partial}{\partial \mathbf{y}'}, 0\right)\boldsymbol{\phi}^{(k-1)}(\mathbf{y}') + \frac{1}{2}\frac{\partial^2 \mathbf{L}}{\partial \Lambda^2}\left(\frac{\partial}{\partial \mathbf{y}'}, 0\right)\boldsymbol{\phi}^{(k-2)}(\mathbf{y}') = \mathbf{0} \ \text{ in } G, \quad (\text{A } 1)$$

$$\mathbf{T}\left(\frac{\partial}{\partial \mathbf{y}'}, 0, \mathbf{n}\right)\boldsymbol{\phi}^{(k)}(\mathbf{y}') + \frac{\partial \mathbf{T}}{\partial \Lambda}\left(\frac{\partial}{\partial \mathbf{y}'}, 0, \mathbf{n}\right)\boldsymbol{\phi}^{(k-1)}(\mathbf{y}') = \mathbf{0} \ \text{ on } \partial G, \quad (\text{A } 2)$$

where we assume that all quantities with negative indices are zero. Furthermore, we notice in the sense of notations (25), (26) that

$$\mathbf{L}_0\left(\frac{\partial}{\partial \mathbf{y}'}\right) = \mathbf{L}\left(\frac{\partial}{\partial \mathbf{y}'}, 0\right), \quad \mathbf{L}_1\left(\frac{\partial}{\partial \mathbf{y}'}\right) = \frac{\partial \mathbf{L}}{\partial \Lambda}\left(\frac{\partial}{\partial \mathbf{y}'}, 0\right), \quad \mathbf{L}_2\left(\frac{\partial}{\partial \mathbf{y}'}\right) = \frac{1}{2}\frac{\partial^2 \mathbf{L}}{\partial \Lambda^2}\left(\frac{\partial}{\partial \mathbf{y}'}, 0\right),$$

$$\mathbf{T}_0\left(\frac{\partial}{\partial \mathbf{y}'}, \mathbf{n}\right) = \mathbf{T}\left(\frac{\partial}{\partial \mathbf{y}'}, 0, \mathbf{n}\right), \quad \mathbf{T}_1(\mathbf{n}) = \frac{\partial \mathbf{T}}{\partial \Lambda}\left(\frac{\partial}{\partial \mathbf{y}'}, 0, \mathbf{n}\right).$$

The 2D boundary value problem (A 1), (A 2) posed on the cross-section G is solvable if and only if the following orthogonality conditions are satisfied:

$$\int_G \left[\frac{\partial \mathbf{L}}{\partial \Lambda}\left(\frac{\partial}{\partial \mathbf{y}'}, 0\right)\boldsymbol{\phi}^{(k-1)}(\mathbf{y}') + \frac{1}{2}\frac{\partial^2 \mathbf{L}}{\partial \Lambda^2}\left(\frac{\partial}{\partial \mathbf{y}'}, 0\right)\boldsymbol{\phi}^{(k-2)}(\mathbf{y}')\right] \cdot \mathbf{R}^{(j)}\, d\mathbf{y}'$$
$$- \int_{\partial G}\left[\frac{\partial \mathbf{T}}{\partial \Lambda}\left(\frac{\partial}{\partial \mathbf{y}'}, 0, \mathbf{n}\right)\boldsymbol{\phi}^{(k-1)}(\mathbf{y}')\right] \cdot \mathbf{R}^{(j)}\, ds = 0, \quad j = 1, 2, 3,$$

where $\mathbf{R}^{(j)}$ are no-trivial solutions of the homogeneous Neumann boundary value problem for the Navier operator in G (i.e. the rigid-body translations and rotations),

$$\mathbf{R}^{(j)} = \mathbf{e}^{(j)}, \quad \mathbf{R}^{(3)} = \mathbf{e}^{(3)} \times \mathbf{y}', \quad j = 1, 2. \quad (\text{A } 3)$$

Finally, we construct a set

$$\{\boldsymbol{\phi}^{(0)}, \boldsymbol{\phi}^{(1)}, \ldots, \boldsymbol{\phi}^{(N)}\}, \quad (\text{A } 4)$$

whose elements are the eigenvector and the generalized eigenvectors of (A 1). We note that the problem (A 1) formulated for $\boldsymbol{\phi}^{(N+1)}$ is not solvable, which means that we can not proceed further in (A 1), (A 2). Often, the set (A 4) is called the Jordan's chain [10],

https://doi.org/10.1017/S0956792599003654 Published online by Cambridge University Press

and the number $N+1$ is said to be the length of Jordan's chain. There are four Jordan's chains

$$\boldsymbol{\phi}^{(k,0)}, \boldsymbol{\phi}^{(k,1)}, \boldsymbol{\phi}^{(k,2)}, \boldsymbol{\phi}^{(k,3)}, \quad k = 1, 2,$$

$$\boldsymbol{\phi}^{(k,0)}, \boldsymbol{\phi}^{(k,1)}, \quad k = 3, 4.$$

Two Jordan's chains of the length 4 correspond to a bending of the cylinder about the Oy_1 or Oy_2 axis, and the remaining chains of the length 2 correspond to a longitudinal tension-compression (in the y_3 direction) and rotation (about the Oy_3 axis). The explicit formulae for $\boldsymbol{\phi}^{(k,j)}$ are

$$\boldsymbol{\phi}^{(1,0)} = \mathbf{e}^{(1)}, \quad \boldsymbol{\phi}^{(2,0)} = \mathbf{e}^{(2)}, \quad \boldsymbol{\phi}^{(3,0)} = \mathbf{e}^{(3)}, \quad \boldsymbol{\phi}^{(4,0)} = -y_2\,\mathbf{e}^{(1)} + y_1\,\mathbf{e}^{(2)},$$

$$\boldsymbol{\phi}^{(1,1)} = -y_1\,\mathbf{e}^{(2)}, \quad \boldsymbol{\phi}^{(2,1)} = -y_2\,\mathbf{e}^{(3)},$$

$$\boldsymbol{\phi}^{(3,1)} = -\frac{\lambda}{2(\mu+\lambda)}\,(y_1\,\mathbf{e}^{(1)} + y_2\,\mathbf{e}^{(2)}), \quad \boldsymbol{\phi}^{(4,1)} = \varphi(y_1, y_2)\,\mathbf{e}^{(3)},$$

$$\boldsymbol{\phi}^{(1,2)} = \frac{\lambda}{4(\mu+\lambda)}\,\{(y_1^2 - y_2^2 - k_1\,y_2)\,\mathbf{e}^{(1)} + (2y_1\,y_2 + k_1\,y_1)\,\mathbf{e}^{(2)}\},$$

$$\boldsymbol{\phi}^{(2,2)} = \frac{\lambda}{4(\mu+\lambda)}\,\{(2y_1\,y_2 - k_2\,y_2)\,\mathbf{e}^{(1)} + (y_2^2 - y_1^2 + k_2\,y_1)\,\mathbf{e}^{(2)}\},$$

$$\boldsymbol{\phi}^{(1,3)} = \mathbf{e}^{(3)}\left\{\frac{4\mu+3\lambda}{12(\mu+\lambda)}\,y_1^3 + \frac{\lambda}{4(\mu+\lambda)}\,y_1\,y_2^2 - \chi_1 + k_1\,\frac{\lambda}{4(\mu+\lambda)}\,\varphi(y_1, y_2)\right\},$$

$$\boldsymbol{\phi}^{(2,3)} = \mathbf{e}^{(3)}\left\{\frac{4\mu+3\lambda}{12(\mu+\lambda)}\,y_2^3 + \frac{\lambda}{4(\mu+\lambda)}\,y_1^2\,y_2 - \chi_2 + k_2\,\frac{\lambda}{4(\mu+\lambda)}\,\varphi(y_1, y_2)\right\}; \tag{A 5}$$

here $\mathbf{e}^{(k)}$ are the unit basis vectors, k_1 and k_2 are constants, and φ, χ_i are the solutions of the following 2D Neumann problems,[3] respectively:

$$\nabla^2\varphi = 0, \quad (y_1, y_2) \in G; \quad \partial_n\,\varphi = y_2\,n_1 - y_1\,n_2, \quad (y_1, y_2) \in \partial G, \tag{A 6}$$

$$\nabla^2\chi_1 = 0, \quad (y_1, y_2) \in G; \quad \partial_n\,\chi_1 = y_1^2\,n_1 + \frac{\lambda}{\lambda+\mu}\,y_1\,y_2\,n_2, \quad (y_1, y_2) \in \partial G, \tag{A 7}$$

$$\nabla^2\chi_2 = 0, \quad (y_1, y_2) \in G; \quad \partial_n\,\chi_2 = y_2^2\,n_2 + \frac{\lambda}{\lambda+\mu}\,y_1\,y_2\,n_1, \quad (y_1, y_2) \in \partial G, \tag{A 8}$$

where the vector $\mathbf{n} = (n_1, n_2)$ is the outward unit normal of ∂G.

The right-hand sides of boundary value problems (A 6), (A 7) and (A 8) are self-balanced, i.e.

$$\int_{\partial G} \partial_n\,\varphi\,ds = 0, \quad \int_{\partial G} \partial_n\,\chi_j\,ds = 0, \quad j = 1, 2,$$

and hence the solvability conditions are satisfied. To provide uniqueness we also impose the normalization conditions

$$\int_G \varphi\,dy_1\,dy_2 = 0, \quad \int_G \chi_j\,dy_1\,dy_2 = 0, \quad j = 1, 2.$$

[3] The functions φ and χ_i are known as torsion and bending potentials [18].

https://doi.org/10.1017/S0956792599003654 Published online by Cambridge University Press

We also note that two constants k_1, k_2 are chosen in such a way that

$$\frac{k_j\,\lambda}{4(\mu+\lambda)}\int_G (\,y_1^2+y_2^2-||\varphi||^2\,)\,dY_1\,dY_2$$

$$=\int_G (\,y_1\,\partial_{y_2}\chi_j-y_2\,\partial_{y_1}\chi_j+(-1)^{j+1}\,\frac{\lambda}{\mu+\lambda}\,y_j\,y_1\,y_2)\,dy_1\,dy_2, \tag{A 9}$$

in order to satisfy certain biorthogonal conditions [7].

The coefficients k_1, k_2 in (A 5) are chosen in accordance with (A 9). Their purpose is to provide two uncoupled differential equations (31) for v_1, v_2. We remark that in the case when (A 9) does not hold, we have to deal with a system of two coupled differential equations with respect to v_1 and v_2.

Appendix A.2 Boundary layer fields

In this section we formulate the boundary value problems for the fields $\mathbf{V}^{(1,0)}(\mathbf{X})$, $\mathbf{V}^{(2,0)}(\mathbf{Y})$ (independent of ε) from the expansion (27).

The above fields compensate for the discrepancy produced by the expansion (28) in the boundary conditions (23), (24) at the ends of the thin cylindrical domain.

The field $\mathbf{V}^{(1,0)}(\mathbf{X})$ is the solution of the following Neumann boundary value problem for the Navier operator

$$\mathbf{L}\left(\frac{\partial}{\partial\mathbf{X}}\right)\mathbf{V}^{(1,0)}(\mathbf{X})=\mathbf{0},\quad(\mathbf{X}_1,\,\mathbf{X}_2)\in G,\quad \mathbf{X}_3>0, \tag{A 10}$$

$$\boldsymbol{\sigma}^{(n)}\left(\frac{\partial}{\partial\mathbf{X}}\right)\mathbf{V}^{(1,0)}(\mathbf{X})=-\mathscr{P}(\mathbf{X}_1,\,\mathbf{X}_2),\quad(\mathbf{X}_1,\,\mathbf{X}_2)\in G,\quad \mathbf{X}_3=0, \tag{A 11}$$

$$\boldsymbol{\sigma}^{(n)}\left(\frac{\partial}{\partial\mathbf{X}}\right)\mathbf{V}^{(1,0)}(\mathbf{X})=\mathbf{0},\quad(\mathbf{X}_1,\,\mathbf{X}_2)\in G,\quad \mathbf{X}_3>0, \tag{A 12}$$

where $\mathscr{P}$ is the leading order approximation of the trace of the vector-function $\boldsymbol{\Psi}^{(0)}$ on the surface $\mathbf{X}_3=0$.

The solution of the problem (A 10)–(A 12), which decays exponentially at infinity, exists only if only [7]

$$\int_G \mathscr{P}\cdot\mathbf{R}^{(j)}\,d\mathbf{X}_1\,d\mathbf{X}_2=0,\quad j=1,\,2,\,3, \tag{A 13}$$

where $\mathbf{R}^{(j)}$ denote the rigid body translations and the rotation about the OX_3 axis (see (A 3)). The conditions (A 13) are equivalent to (35).

The field $\mathbf{V}^{(2,0)}(\mathbf{Y})$ satisfies the mixed Dirichlet–Neumann boundary value problem for the Navier operator

$$\mathbf{L}\left(\frac{\partial}{\partial\mathbf{Y}}\right)\mathbf{V}^{(2,0)}(\mathbf{Y})=\mathbf{0},\quad(\mathbf{Y}_1,\,\mathbf{Y}_2)\in G,\quad \mathbf{Y}_3<0, \tag{A 14}$$

$$\boldsymbol{\sigma}^{(n)}\left(\frac{\partial}{\partial\mathbf{Y}}\right)\mathbf{V}^{(2,0)}(\mathbf{Y})=\mathbf{0},\quad(\mathbf{Y}_1,\,\mathbf{Y}_2)\in G,\quad \mathbf{Y}_3<0, \tag{A 15}$$

$$\mathbf{V}^{(2,0)}(\mathbf{Y})=-\mathbf{Q}(\mathbf{Y}_1,\,\mathbf{Y}_2),\quad(\mathbf{Y}_1,\,\mathbf{Y}_2)\in G,\quad \mathbf{Y}_3=0, \tag{A 16}$$

https://doi.org/10.1017/S0956792599003654 Published online by Cambridge University Press

where $\mathbf{Q}$ represents the leading order approximation of the discrepance produced by $\boldsymbol{\Psi}^{(0)}$ in the boundary condition (23).

The conditions for the exponential decay of $\mathbf{V}^{(2,0)}$ have the form (34) (for more details see [7]). We remark that in our simple example the formula (34) yields $\mathbf{Q} \equiv 0$ and $\mathbf{V}^{(2,0)} \equiv 0$.

Appendix A.3 Homogenisation of the linear elasticity equations

For the sake of reader's convenience, we give a brief description of the homogenization procedure for the Navier system (the general theory is given by Bakhvalov & Panasenko [16]).

$$\mathscr{L}_{xx}(\mathbf{u}) := \mu\Delta\mathbf{u} + (\lambda+\mu)\nabla\nabla\cdot\mathbf{u} = \mathbf{0}, \quad \mathbf{x}\in\Omega. \tag{A 17}$$

The displacement vector $\mathbf{u}$ depends on the 'slow' variables $\mathbf{x}$ and the 'fast' variables $\boldsymbol{\xi} = \mathbf{x}/\varepsilon$. Fast coordinates are associated with the periodic structure (containing inclusions, cavities, etc.) characterized by the small parameter ε. The differential operator of the 2D Navier system can be rewritten in the matrix form:

$$\mathscr{L}_{tx} := \mathscr{D}_{\frac{\partial}{\partial t}}\mathscr{H}(\xi)\mathscr{D}^t_{\frac{\partial}{\partial x}}, \tag{A 18}$$

where

$$\mathscr{D}_{\frac{\partial}{\partial x}} = \begin{pmatrix} \dfrac{\partial}{\partial x_1} & 0 & \dfrac{1}{\sqrt{2}}\dfrac{\partial}{\partial x_2} \\ 0 & \dfrac{\partial}{\partial x_2} & \dfrac{1}{\sqrt{2}}\dfrac{\partial}{\partial x_1} \end{pmatrix} \quad \mathscr{H} = \begin{pmatrix} 2\mu+\lambda & \lambda & 0 \\ \lambda & 2\mu+\lambda & 0 \\ 0 & 0 & 2\mu \end{pmatrix}.$$

We are looking for a solution of the Navier system $\mathscr{L}_{xx}\,\mathbf{u}(\mathbf{x},\boldsymbol{\xi}) = 0$ in the following asymptotic form:

$$\mathbf{u}(\mathbf{x},\,\boldsymbol{\xi}) = \mathbf{u}^{(0)}(\mathbf{x}) + \varepsilon\mathbf{u}^{(1)}(\mathbf{x},\,\xi) + \varepsilon^2\,\mathbf{u}^{(2)}(\mathbf{x},\,\xi) + O(\varepsilon^3). \tag{A 19}$$

The coefficients in (A 19) solve the recurrent system of equations:

$$\mathscr{L}_{\xi\xi}\,\mathbf{u}^{(0)}(\mathbf{x}) = \mathbf{0}, \tag{A 20}$$

$$\mathscr{L}_{\xi\xi}\,\mathbf{u}^{(1)}(\mathbf{x},\,\boldsymbol{\xi}) = -\mathscr{L}_{\xi x}\,\mathbf{u}^{(0)}(\mathbf{x}) - \mathscr{L}_{x\xi}\,\mathbf{u}^{(0)}(\mathbf{x}), \tag{A 21}$$

$$\mathscr{L}_{\xi\xi}\,\mathbf{u}^{(2)}(\mathbf{x},\,\boldsymbol{\xi}) = -\mathscr{L}_{\xi x}\,\mathbf{u}^{(1)}(\mathbf{x},\,\boldsymbol{\xi}) - \mathscr{L}_{x\xi}\,\mathbf{u}^{(1)}(\mathbf{x},\,\boldsymbol{\xi}) - \mathscr{L}_{xx}\,\mathbf{u}^{(0)}(\mathbf{x}). \tag{A 22}$$

The first equation (A 20) is the identity. Note, that $\mathscr{L}_{x\xi}\,\mathbf{u}^{(0)}(\mathbf{x}) = 0$ as well. The right hand side of the equation (A 21) can be simplified as

$$\begin{aligned}\mathscr{L}_{\xi x}\,\mathbf{u}^{(0)}(\mathbf{x}) &= \mathscr{D}_{\frac{\partial}{\partial\xi}}\mathscr{H}(\xi)\mathscr{D}^t_{\frac{\partial}{\partial x}}\,\mathbf{u}^{(0)} = \mathscr{D}_{\frac{\partial}{\partial\xi}}\mathscr{H}(\xi)\left(\frac{\partial u_0}{\partial x_1},\quad \frac{\partial v_0}{\partial x_2},\quad \frac{1}{\sqrt{2}}\left(\frac{\partial u_0}{\partial x_2}+\frac{\partial v_0}{\partial x_1}\right)\right) \\ &= \sum_{n=1}^{3} C_n(\mathbf{x})\,\mathscr{D}_{\frac{\partial}{\partial\xi}}\mathscr{H}(\xi)\mathscr{D}^t_{\frac{\partial}{\partial\xi}}\mathbf{V}^{(n)} = \sum_{n=1}^{3} C_n(\mathbf{x})\mathscr{L}_{\xi\xi}\,\mathbf{V}^{(n)}.\end{aligned} \tag{A 23}$$

https://doi.org/10.1017/S0956792599003654 Published online by Cambridge University Press

Here we use the following notations:

$$\mathbf{u}^{(0)} = \begin{pmatrix} u_0 \\ v_0 \end{pmatrix}, \quad C_1(\mathbf{x}) = \frac{\partial u_0}{\partial x_1}, \quad C_2(\mathbf{x}) = \frac{\partial v_0}{\partial x_2}, \quad C_3(\mathbf{x}) = \frac{1}{\sqrt{2}}\left(\frac{\partial u_0}{\partial x_2} + \frac{\partial v_0}{\partial x_1}\right),$$

$$\mathbf{V}^{(1)} = \begin{pmatrix} \xi_1 \\ 0 \end{pmatrix}, \quad \mathbf{V}^{(2)} = \begin{pmatrix} 0 \\ \xi_2 \end{pmatrix}, \quad \mathbf{V}^{(3)} = \frac{1}{\sqrt{2}}\begin{pmatrix} \xi_2 \\ \xi_1 \end{pmatrix}, \quad \mathscr{D}^t_{\frac{\partial}{\partial \xi}}\mathbf{V}^{(n)} = \begin{pmatrix} \delta_{1n} \\ \delta_{2n} \\ \delta_{3n} \end{pmatrix}.$$

It is easy to see that

$$\mathbf{u}^{(1)}(\mathbf{x}, \boldsymbol{\xi}) = \sum_{n=1}^{3} \mathbf{W}^{(n)}(\xi)\, C_n(\mathbf{x}), \tag{A 24}$$

where the fields $\mathbf{W}^{(n)}$ satisfy the following system:

$$\mathscr{L}_{\xi\xi}(\mathbf{W}^{(n)}(\xi) + \mathbf{V}^{(n)}(\xi)) = \mathbf{0}, \quad \mathbf{x} \in \mathbb{R}^2. \tag{A 25}$$

It has a solution if and only if the following solvability conditions hold:

$$\langle \boldsymbol{\xi} \times \mathbf{L}_{\xi\xi}\, \mathbf{u}^{(i)} \rangle = \mathbf{0} \quad \text{and} \quad \langle \mathbf{L}_{\xi\xi}\, \mathbf{u}^{(i)} \rangle = \mathbf{0}, \tag{A 26}$$

where $\langle \cdot \rangle$ denotes the average over an elementary cell of the periodic structure. We apply the condition (A 26) to each elementary cell separately and obtain the periodicity boundary conditions for the functions $\mathbf{W}^{(n)}$. In the case of the square periodical cell $[1 \times 1]$ the 'periodical boundary conditions' can be formulated as

$$\mathbf{W}^{(n)}(0, \xi_2) = \mathbf{W}^{(n)}(1, \xi_2), \quad \sigma(\mathbf{W}^{(n)}; 0, \xi_2) = \sigma(\mathbf{W}^{(n)}; 1, \xi_2), \tag{A 27}$$

$$\mathbf{W}^{(n)}(\xi_1, 0) = \mathbf{W}^{(n)}(\xi_1, 1), \quad \sigma(\mathbf{W}^{(n)}; \xi_1, 0) = \sigma(\mathbf{W}^{(n)}; \xi_1, 1). \tag{A 28}$$

Now consider the third equation (A 22). Employing the following useful notations

$$\mathbf{W} = \begin{pmatrix} \mathbf{W}_1^{(1)} & \mathbf{W}_1^{(2)} & \mathbf{W}_1^{(3)} \\ \mathbf{W}_2^{(1)} & \mathbf{W}_2^{(2)} & \mathbf{W}_2^{(3)} \end{pmatrix}, \quad \mathbf{V} = \begin{pmatrix} \mathbf{V}_1^{(1)} & \mathbf{V}_1^{(2)} & \mathbf{V}_1^{(3)} \\ \mathbf{V}_2^{(1)} & \mathbf{V}_2^{(2)} & \mathbf{V}_2^{(3)} \end{pmatrix}, \quad \mathbf{C} = (\, C_1 \quad C_2 \quad C_3\,)^t,$$

we write the right-hand side of the equation (A 22) as

$$\begin{aligned} &\mathscr{D}_{\frac{\partial}{\partial \xi}} \mathscr{H}(\xi)\, \mathscr{D}^t_{\frac{\partial}{\partial x}} \mathbf{W}(\boldsymbol{\xi})\, \mathbf{C}(\mathbf{x}) + \mathscr{D}_{\frac{\partial}{\partial x}} \mathscr{H}(\xi)\, \mathscr{D}^t_{\frac{\partial}{\partial \xi}} \mathbf{W}(\boldsymbol{\xi})\, \mathbf{C}(\mathbf{x}) + \mathscr{D}_{\frac{\partial}{\partial \xi}} \mathscr{H}(\xi)\, \mathbf{C}(\mathbf{x}) \\ &= \mathscr{D}_{\frac{\partial}{\partial \xi}} \mathscr{H}(\xi)\, \mathbf{W}^t(\boldsymbol{\xi})\, \mathscr{D}_{\frac{\partial}{\partial x}}\, \mathscr{D}^t_{\frac{\partial}{\partial x}} \mathbf{u}^{(0)}(\mathbf{x}) + \mathscr{D}_{\frac{\partial}{\partial x}} \left(\mathscr{H}(\xi)\, \mathscr{D}^t_{\frac{\partial}{\partial \xi}} \{\mathbf{W}(\boldsymbol{\xi}) + \mathbf{V}(\boldsymbol{\xi})\} \right) \mathscr{D}^t_{\frac{\partial}{\partial x}} \mathbf{u}^{(0)}(\mathbf{x}). \end{aligned} \tag{A 29}$$

Now apply the solvability conditions (A 26). The first term in (A 29) vanishes due to the periodicity boundary conditions imposed on the function $\mathbf{W}^{(n)}$. The second one gives the homogenized elasticity equation

$$\mathscr{D}_{\frac{\partial}{\partial x}} \widehat{\mathscr{H}} \mathscr{D}^t_{\frac{\partial}{\partial x}} \mathbf{u}^{(0)}(\mathbf{x}) = \mathbf{0}, \quad \mathbf{x} \in \Omega, \tag{A 30}$$

and the expression for the matrix of effective elastic moduli

$$\widehat{\mathscr{H}} = \int_{[1\times 1]} \mathscr{H}(\xi)\, \mathscr{D}^t_{\frac{\partial}{\partial \xi}} \{\mathbf{W}(\boldsymbol{\xi}) + \mathbf{V}(\boldsymbol{\xi})\}\, d\mathbf{x}. \tag{A 31}$$

It is verified by direct calculations that

$$\mathscr{H}(\mathbf{x})\, \mathscr{D}^t_{\frac{\partial}{\partial \xi}} \{\mathbf{W}(\boldsymbol{\xi}) + \mathbf{V}(\boldsymbol{\xi})\} = \begin{pmatrix} \boldsymbol{\sigma}_{11} \\ \boldsymbol{\sigma}_{22} \\ \sqrt{2}\,\boldsymbol{\sigma}_{12} \end{pmatrix} = \boldsymbol{\sigma}, \quad \mathscr{D}^t_{\frac{\partial}{\partial \xi}} \{\mathbf{W}(\boldsymbol{\xi}) + \mathbf{V}(\boldsymbol{\xi})\} = \begin{pmatrix} \boldsymbol{\varepsilon}_{11} \\ \boldsymbol{\varepsilon}_{22} \\ \sqrt{2}\,\boldsymbol{\varepsilon}_{12} \end{pmatrix} = \boldsymbol{\varepsilon}$$

https://doi.org/10.1017/S0956792599003654 Published online by Cambridge University Press

and the final relation (A 31) can be rewritten in the following form:

$$\widehat{\mathbf{H}} = \int_{[1\times 1]} [\mathbf{H}(\boldsymbol{\xi})\, \mathscr{D}^t_{\frac{\partial}{\partial \xi}} \{\mathbf{W}(\boldsymbol{\xi}) + \mathbf{V}(\boldsymbol{\xi})\}]^t \mathscr{D}^t_{\frac{\partial}{\partial \xi}} \{\mathbf{W}(\boldsymbol{\xi}) + \mathbf{V}(\boldsymbol{\xi})\}\, d\mathbf{x}$$

$$= \int_{[1\times 1]} \boldsymbol{\sigma}^t(\mathbf{W}(\boldsymbol{\xi}) + \mathbf{V}(\boldsymbol{\xi}))\, \boldsymbol{\varepsilon}(\mathbf{W}(\boldsymbol{\xi}) + \mathbf{V}(\boldsymbol{\xi}))\, d\mathbf{x} \tag{A 32}$$

Appendix A.4 Asymptotic expansion of the solution in the thin bridge

In this section we analyse the solution of linear isotropic elasticity in thin region. Such kind of problem was firstly solved by Mouchan & Mouchan [19] and here we rewrite the general procedure as this solution is important for analysis honeycomb structures (see § 5). The mathematical formulation of the problem can be formulated as

$$\mathscr{L}_{xx}(\mathbf{u};\mathbf{x}) := \mathscr{D}_{\frac{\partial}{\partial x}} \mathscr{H}(\xi)\, \mathscr{D}^t_{\frac{\partial}{\partial x}}(\mathbf{U}) = \mathbf{0}, \quad \mathbf{x} \in \Omega,$$

$$\boldsymbol{\sigma}^{(n)}(\mathbf{U};\mathbf{x}) = \begin{pmatrix} p^{(1)}_{\pm} \\ \varepsilon^2\, p^{(2)}_{\pm} \end{pmatrix}, \quad \mathbf{x} \in \partial\Omega^{(1)}; \quad \mathbf{U} = \mathbf{a}_{\pm}, \quad \mathbf{x} \in \partial\Omega^{(2)}, \tag{A 33}$$

where

$$\mathscr{D}_{\frac{\partial}{\partial x}} = \begin{pmatrix} \dfrac{\partial}{\partial x_1} & 0 & \dfrac{1}{\sqrt{2}}\dfrac{\partial}{\partial x_2} \\ 0 & \dfrac{\partial}{\partial x_2} & \dfrac{1}{\sqrt{2}}\dfrac{\partial}{\partial x_1} \end{pmatrix} \quad \mathscr{H} = \begin{pmatrix} 2\mu+\lambda & \lambda & 0 \\ \lambda & 2\mu+\lambda & 0 \\ 0 & 0 & 2\mu \end{pmatrix}$$

and $\Omega = \{(x, \varepsilon t) : -1 < x < 1, -\frac{1}{2} < t < \frac{1}{2}\}$, $\partial\Omega^{(1)} = \{t = \pm\frac{1}{2}\}$, $\partial\Omega^{(2)} = \{x = \pm 1\}$.

Due to the presence of the small parameter ε, which is the thickness of the thin bridge we can rewrite the Navier system in the stretched coordinates x, t and define the recursive identities for the displacement vector:

$$\partial^2_{tt}\, U^{(n)}_1 = -\frac{\lambda+\mu}{\mu}\, \partial^2\, U^{(n-1)}_2 - \frac{\lambda+2\mu}{\mu}\, \partial^2_{xx}\, U^{(n-2)}_1, \quad |t| < 1/2,$$

$$\partial_t\, U^{(n)}_1 = -\partial_x\, U^{(n-1)}_2, \quad |t| = \pm 1/2,$$

$$\partial^2_{tt}\, U^{(n)}_2 = -\frac{\lambda+\mu}{\lambda+2\mu}\, \partial^2\, U^{(n-1)}_1 - \frac{\mu}{\lambda+2\mu}\, \partial^2_{xx}\, U^{(n-2)}_2, \quad |t| < 1/2,$$

$$\partial_t\, U^{(n)}_2 = -\frac{\lambda}{\lambda+2\mu}\, \partial_x\, U^{(n-1)}_1, \quad |t| = \pm 1/2. \tag{A 34}$$

Now we apply the formulae (A 34) and check the solvability conditions on each step. These procedure gives us the full asymptotic expansion of the solution (A 33). It admits the following form:

$$\mathbf{u} = \sum_{i=0}^{\infty} \varepsilon^i \left[\sum_{n=0}^{2} \varepsilon^n\, \mathscr{U}^{(n)}_i + \sum_{n=0}^{4} \varepsilon^n\, \mathscr{V}^{(n)}_i \right]. \tag{A 35}$$

It is possible to see that this solution includes two set of Jordan chains. One corresponds to the leading term with longitudinal components of the displacement, and another has the transversal displacement in the leading term. The first Jordan chain has the following

https://doi.org/10.1017/S0956792599003654 Published online by Cambridge University Press

form:

$$\mathscr{U}^{(0)} = \begin{pmatrix} u_0 \\ 0 \end{pmatrix}, \quad \mathscr{U}^{(1)} = \begin{pmatrix} 0 \\ -\dfrac{\lambda}{\lambda+2\mu}\, t\, \partial_x u_0 \end{pmatrix}, \quad \mathscr{U}^{(2)} = \begin{pmatrix} \dfrac{\lambda}{\lambda+2\mu}\, \dfrac{t^2}{2}\, \partial_x^2 u_0 + \mathscr{U} \\ 0 \end{pmatrix},$$

where $\mathscr{U}$ is the solution of the following boundary value problem:

$$\begin{aligned} \partial_t^2 \mathscr{U} &= -\frac{4(\lambda+\mu)}{\lambda+2\mu}\, \partial_x^2 u_0, \quad |t| < 1/2, \\ \partial_t \mathscr{U} &= \frac{1}{\mu}\, p_{\pm}^{(1)}, \quad t = \pm 1/2. \end{aligned} \tag{A 36}$$

The solvability condition of the system (A 36) gives us the equation for the leading term of the longitudinal displacement:

$$-\frac{4(\lambda+\mu)}{\lambda+2\mu}\, \partial_x^2 u_0 = p_+^{(1)} - p_-^{(1)}.$$

For the case of free-traction lateral surfaces, the leading term of the longitudinal displacement is the linear polynomial function.

The second Jordan chain describing the leading transversal displacement has the following form:

$$\mathscr{V}^{(0)} = \begin{pmatrix} 0 \\ v_0 \end{pmatrix}, \quad \mathscr{V}^{(1)} = \begin{pmatrix} -t\, \partial_x v_0 \\ 0 \end{pmatrix}, \quad \mathscr{V}^{(2)} = \begin{pmatrix} 0 \\ \dfrac{\lambda}{\lambda+2\mu}\, \dfrac{t^2}{2}\, \partial_x^2 v_0 \end{pmatrix},$$

$$\mathscr{V}^{(3)} = \begin{pmatrix} \left[\dfrac{4\mu+3\lambda}{6(\lambda+2\mu)}\, t^3 - \dfrac{\lambda+\mu}{2(\lambda+2\mu)}\, t \right] \partial_x^3 v_0 \\ 0 \end{pmatrix},$$

$$\mathscr{V}^{(4)} = \begin{pmatrix} 0 \\ \left[-\dfrac{3\lambda+2\mu}{24(\lambda+2\mu)}\, t^4 + \dfrac{(\lambda+\mu)(3\lambda+\mu)}{12(\lambda+2\mu)^2}\, t^2 \right] \partial_x^4 v_0 + \mathscr{V} \end{pmatrix},$$

where $\mathscr{V}$ satisfies the equations:

$$\begin{aligned} \partial_t^2 \mathscr{V} &= \frac{\mu(\lambda+\mu)}{3(\lambda+2\mu)^2}\, \partial_x^4 v_0, \\ \partial_t \mathscr{V} &= \frac{1}{\lambda+2\mu}\, p_{\pm}^{(2)}. \end{aligned} \tag{A 37}$$

From the solvability condition, we derive the equation for the leading term of the transversal displacement:

$$\frac{\mu(\lambda+\mu)}{3(\lambda+2\mu)}\, \partial_x^4 v_0 = \varepsilon(p_+^{(2)} - p_-^{(2)}).$$

Note that in the case of free-traction lateral surfaces, the transversal displacement is specified by the cubic polynomial.

https://doi.org/10.1017/S0956792599003654 Published online by Cambridge University Press

References

[1] Kolaczkowski, S. T. (1995) Catalytic stationary gas turbine combustors: a review of the challenges faced to clear the next set of hurdles. *Trans. IChemE, Part A*. **73**, 168–190; Erratum, *Part A*, **73**, 865.

[2] Hayes, R. E. & Kolaczkowski, S. T. (1997) *Introduction to Catalytic Combustion*. Gordon and Breach.

[3] Furuya, A., Nishida, T. & Matsuhisa, T. (1994) Thermal stress analysis for high temperature combustion catalyst honeycomb. *Proc. Intl Workshop on Catalytic Combustion*.

[4] Adshead-Farey, S. M. (1994) Private communication and access to a report commissioned by Rolls Royce IMGT Ltd on: *Thermal stress analysis of a washcoated catalytic combustor monolith – Task 6, by Frazer-Nash Consultancy Ltd, TR04*.

[5] Hunt, H. E. M. (1993) The mechanical strength of ceramic honeycomb monoliths as determined by simple experiments. *Trans. IChemE. Part A*, **71**, 257–266.

[6] Florence, A. L. & Simons, J. W. (1992) Development of durable temperature catalysts for natural gas combustion – Analysis of thermal stresses in combustion catalysts monoliths. *Gas Research Institute, Technical Report GRI-92/0399*.

[7] Kozlov, V. K., Maz'ya, V. G. & Movchan, A. B. (1995) Asymptotic representation of elastic fields in a multi-structure. *Asymptotic Analysis*, **11**, 343–415.

[8] Nowacki, W. (1975) *Dynamic Problems of Thermoelasticity*. Polish Scientific Publishers.

[9] Kozlov, V. K., Maz'ya, V. G. & Movchan, A. B. (1994) Asymptotic analysis of a mixed boundary value problem in a multi-structure. *Asymptotic Analysis*, **8**, 105–143.

[10] Maz'ya, V. G., Nazarov, S. A. & Plamenevskii, B. A. (1991/92) *Asymptotische Theorie Elliptischer Randwertanfgaben in Singulär Gestörten*. Akademie-Verlag, Berlin, B.1, 1991; B.2, 1992.

[11] Arutyunyan, N. Kh., Movchan, A. B. & Nazarov, S. A. (1987) *Advances in Mechanics*, **10**, 3–91.

[12] Shkalikov, A. A. & Shkred, A. B. (1991) *Matem. Sbornik*, **3**, 1222–1246.

[13] Williams, M. L. (1952) Stress singularities resulting from various boundary conditions in angular corner of plate in extension. *J. Appl. Mech.*, **19**.

[14] Gibson, L. J. & Ashby, M. (1998) *Cellular Solids*. Pergamon Press.

[15] Torquato, S., Gibiansky, L. V., Silva, M. A. & Gibson, L. J. (1998) Effective mechanical and transport properties of cellular solids.

[16] Bakhvalov, N. S. & Panasenko, G. P. (1989) *Homogenization: Averaging Processes in Periodic Media*. Kluwer.

[17] Nemat-Nasser, S. & Hori, M. (1993) *Micromechanics: Overall Properties of Heterogeneous Solids*. North-Holland.

[18] Lurie, A. I. (1970) *Theory of Elasticity*. Nauka, Moscow.

[19] Movchan, A. B. & Movchan, N. V. (1995) *Mathematical Modelling of Solids with Nonregular Boundaries*. CRC Press.